Role of Reactive Sulfur Species in Mitochondrial Quality Control and Ischemic Stress Resistance in Rodent Hearts

Shimoda, Kakeru

The Graduate University for Advanced Studies, SOKENDAI

School of Life Science

Department of Physiological Sciences

Table of Contents

Abstract

Mitochondria are the organelles that produce adenosine 5'-triphosphate, the major energy molecule for cardiomyocytes, utilizing highly redox (reduction-oxidation)-dependent oxidative phosphorylation system. Mitochondria constantly undergo fission and fusion to maintain their integrity, which is critical for cardiac energy homeostasis and physiological function. In failing hearts, mitochondria in the cardiomyocytes are often found to be fragmented, and accumulating evidence suggests that mitigating mitochondrial hyperfission during heart failure ameliorates cardiac function. However, its molecular mechanism and practical therapeutic approach remain to be fully elucidated.

In the first section, I examined the effect of cilnidipine, one of the approved anti-hypertensive drugs, on mitochondrial fragmentation induced by myocardial infarction (MI) in mice, based on our previous *in vitro* study showing that cilnidipine decreased mitochondrial fragmentation after hypoxic stress. I revealed that treatment of cilnidipine after MI improved cardiac contractile dysfunction along with suppressing mitochondrial fragmentation, suggesting that the maintenance of mitochondrial quality control by cilnidipine treatment can be an attractive therapeutics for ischemic heart failure.

In the second section, I investigated the pathophysiological role of redox-dependent mitochondrial fragmentation in mouse hearts. Our laboratory newly found that dynamin-related protein 1 (Drp1) changes its activity for promoting mitochondrial fission depending on the redox modification on its cysteine residue, such as polysulfidation and depolysulfidation. Indeed, methylmercury (MeHg), an environmental potent electrophile that is known as a cause of Minamata disease with severe neurotoxicity, induces depolysulfidation of polysulfidated Drp1, thereby activating Drp1, promoting

1

mitochondrial hyperfission, and exacerbating pressure overload-induced heart failure. Moreover, sulfide donor restores Drp1 polysulfidation. To test whether polysulfidation state of Drp1 is a risk factor for cardiac diseases, I examined the effect of sulfide donor on the pressure overload-induced heart failure model *in vivo* where the cardiac function was worsened by MeHg exposure. I found that treatment of sulfide donor sodium hydrogen sulfide rescued MeHg-induced cardiac vulnerability to pressure overload, suggesting that modification of Drp1 polysulfidation is important for mitochondrial quality control and cardiac robustness.

Protein polysulfidation is mediated by reactive sulfur species (RSS), which have highly reactive sulfur atoms. Due to its high reactivity, it has been suggested that RSS have important roles not only in protein polysulfidation but also in highly redox-active mitochondrial respiration, which means RSS may have critical role for maintaining mitochondrial function during the myocardial ischemic stress. Therefore, I focused on the contribution of RSS to myocardial ischemic stress resistance. This study revealed that RSS level was decreased in myocardial ischemia reperfusion (I/R) injury in mice. In neonatal rat cardiomyocytes (NRCMs), hypoxic stress-induced RSS decrease was accompanied with increase in hydrogen sulfide (H_2S), suggesting that RSS were reduced to H_2S under hypoxic condition. Treatment of RSS donor sodium tetrasulfide recovered cardiac function in I/R-induced heart failure, indicating that RSS is protective against cardiac ischemic stress. mRNA level of cysteinyl aminoacyl tRNA synthetase (CARS) 2 that is one of the RSS-producing enzymes was found to be decreased after I/R injury. Moreover, CARS2 heterozygous deleted mice were more vulnerable to I/R injury, where cardiac RSS level was significantly decreased compared to wild type mice, suggesting that RSS synthesized by CARS2 contribute to cardiac ischemic stress resistance.

2

Moreover, CARS2 knockdown in NRCMs declined mitochondrial membrane potential after hypoxic stress, indicating that CARS2 is required for maintenance of mitochondrial function during hypoxic stress. I also found that mRNA level of RSS-catabolizing enzymes was decreased in I/R-injured hearts. Furthermore, it was revealed that mRNA level of cytosolic isoform of CARS2, CARS1, was increased in I/R-injured hearts. These results suggest that overall RSS synthesis and catabolism in cells contribute to ischemic stress resistance.

Collectively, these results suggest that RSS synthesis and catabolism contribute to cardiac homeostasis through protein polysulfidation and the maintenance of mitochondrial quality control, thereby inducing cardioprotective effect. The present study proposes that RSS are the key factors, along with reactive oxygen species and reactive nitrogen species, for understanding the molecular mechanism of cardiac pathophysiology. Moreover, this study suggests that the contribution of RSS to mitochondrial respiration (sulfur respiration) in the heart, proposing new insights for cardiac redox biology.

Abbreviation

3-MST	3-Mercaptopyruvate sulfurtransferase
ATP	Adenosine 5'-triphosphate
CARS	Cysteinyl aminoacyl tRNA synthetase
CBS	Cystathionine β-synthase
CSE	Cystathionine ɤ-lyase
Cys-SH	L-cysteine
Cys-SSH	Cysteine persulfide
Drp1	Dynamin-related protein 1
ETHE1	Persulfide dioxygenase
I/R	Ischemia reperfusion
Mfn	Mitofusin
MI	Myocardial infarction
Opa1	Optic atrophy 1
OXPHOS	Oxidative phosphorylation
ROS	Reactive oxygen species
RSS	Reactive sulfur species
SQOR	Sulfide:quinone oxidoreductase
SUOX	Sulfite oxidase
TAC	Transverse aortic constriction
TST	Thiosulfate sulfurtransferase

Introduction

Mitochondrial quality control in the heart

      The heart is continuously beating and therefore, consumes large amount of adenosine 5'-triphosphate (ATP). To meet this high energy demand, mitochondrial oxidative phosphorylation (OXPHOS) is used to generate ATP effectively (Figure 1A). As most of the ATP production in the heart is derived from mitochondrial OXPHOS system[1], mitochondria are important for cardiac energy homeostasis. Indeed, mitochondrial dysfunction is related to several heart diseases. In rat heart failure model induced by aortic stenosis, the expression of mRNA encoding mitochondrial respiratory chain is decreased and mitochondrial function is impaired[2].

      In OXPHOS system, proton gradient between mitochondrial matrix and intermembrane space is generated by reduction-oxidation (redox) reaction for production of ATP[3] (Figure 1A). This highly reactive system can produce reactive oxygen species (ROS) as byproduct[3]. Although ROS-scavenging system is present in the mitochondria, the ability to scavenge ROS does not meet the level of ROS produced in mitochondria[4]. Increase of ROS induces peroxidation of lipid and oxidation of proteins which contribute to respiratory chain, and these cause mitochondrial dysfunction[5]. To maintain mitochondrial function under this severe condition, cells are equipped with mitochondrial quality control system. One important mechanism of mitochondrial quality control is regulation of mitochondrial dynamics, mitochondrial fission and fusion. Mitochondrial dynamics is regulated by several GTPases, dynamin-related protein 1 (Drp1) for fission and mitofusin 1/2 (Mfn1/2) and optic atrophy 1 (Opa1) for fusion[6,7]. Regulation of mitochondrial dynamics is important for cardiac homeostasis. For example, deletion of

Drp1 induces elongation and dysfunction of mitochondria, left ventricular remodeling, and cardiac dysfunction[8]. Interestingly, depletion of Mfn1/2, which induces mitochondrial fragmentation, also causes cardiac dysfunction[9]. These reports suggest that imbalance of mitochondrial fusion/fission is toxic for the heart. Indeed, Drp1/Mfn1/2 triple knockout (KO) mice that have no mitochondrial dynamics, are less toxic for the heart compared to Drp1 single KO mice or Mfn1/2 double KO mice that have imbalanced mitochondrial dynamics[10]. Therefore, mitochondrial dynamics (balance between fusion/fission) must be strictly regulated for maintenance of cardiac robustness and can be therapeutic target for heart failure. Particularly, as mitochondrial fragmentation is observed in failing hearts including myocardial infarction (MI)[11], methylmercury (MeHg)-induced cardiotoxicity[12], high fat diet-induced cardiac dysfunction[13], and aortic stenosis [transverse aortic constriction (TAC)]-induced heart failure[14], suppressing mitochondrial hyperfission is considered to be reasonable therapeutic target for heart failure. Our group previously found that cilnidipine, anti-hypertensive drug approved in Japan, suppressed mitochondrial fragmentation caused by hypoxic stress in neonatal rat cardiac fibroblasts[11]. However, it had been unknown whether cilnidipine actually improves *in vivo* heart failure after ischemia.

Redox-dependent regulation of mitochondrial dynamics through reactive sulfur species

Mitochondrial dynamics is regulated by redox reaction. Especially, Drp1 is known as redox-sensitive protein, and the activity is regulated by redox modification of the cysteine residue such as sulfenylation[15] and S-nitrosylation[16]. Therefore, cysteine-based redox reaction can be important for mitochondrial and cardiovascular homeostasis

and changes in redox status of Drp1 can cause cardiovascular disease. One of the well-known redox modifiers is environmental chemical MeHg. Because MeHg can stably bind to thiol group and change the function of proteins[17], accumulation in high dose of MeHg in organisms induces neurotoxicity such as Minamata disease[18]. In addition, low dose of MeHg, which is considered as sub-neurotoxic dose, increase the cardiac risk[19]. This report indicates that MeHg can affect more strikingly to cardiovascular system than central nervous system. Recently, our group reported that cysteine residue of Drp1 was polysulfidated[12]. Moreover, MeHg depolysulfidated and activated Drp1 and exacerbated pressure overload-induced heart failure[12] (Figure 1B). Although these results suggest that modulation of Drp1 polysulfidation can be therapeutic target for MeHg-induced cardiac vulnerability, such strategy had not been demonstrated.

These observations described above imply physiological importance of redox modification at cysteine thiol group (Figure 1), especially protein polysulfidation. Recently, it is reported that many cysteine residues in proteins are polysufidated at the translational phase[20], indicating that cysteine polysulfidation can be universal phenomena. Protein polysulfidation is also mediated by trans-sulfidation from small molecules such as cysteine persulfide (Cys-SSH) and glutathione persulfide (GSSH)[21]. These persulfides contain sulfane sulfur, sulfur atom which has six valence electrons with no charge[22], which makes persulfides highly reactive. Thus, these molecules which have sulfane sulfur are referred as reactive sulfur species (RSS)[23]. RSS have higher nucleophilicity compared to corresponding thiol (Table 1), and also electrophilicity, while thiol is not electrophilic[23]. Because of this chemical nature of RSS, they are thought to be a more redox-active than corresponding thiol and have central role in redox reaction for proteins and mitochondria. However, the role of RSS in the heart is largely unknown.

Several enzymes can catalyze synthesize of RSS. Previous study demonstrated that cystathionine β-synthase (CBS) and cystathionine ɤ-lyase (CSE) utilized cystine (CysS-SCys) as substrate to produce Cys-SSH[24]. However, as the expression level of these enzymes is very low in the heart[25], they cannot be main RSS-producing enzyme in the heart. Recent report showed that cysteinyl aminoacyl tRNA synthetase (CARS) 2 could generate Cys-SSH using L-cysteine (Cys-SH) as substrate in mouse tissue[20]. Therefore, CARS2 can be the principal generator of RSS in the heart. However, the role of CARS2 in the heart have not been revealed.

In this study, three topics are examined and discussed. First, the effects of cilnidipine on mouse MI model were checked. Intraperitoneal administration of cilnidipine improved cardiac function and mitochondrial fragmentation after MI, suggesting that mitochondrial quality control can be new therapeutic strategy for heart failure. Second, it was tested whether modulation of Drp1 polysulfidation can be therapeutic target for MeHg-induced cardiac vulnerability to pressure overload. Treatment of sulfide donor sodium hydrogen sulfide (NaHS) suppressed MeHg-induced cardiac vulnerability. As our previous study showed that MeHg decreased Drp1 polysulfidation and NaHS recovered Drp1 polysulfidation[12], this result indicates that the cysteine residues of Drp1 susceptible to polysulfidation can be important therapeutic target for MeHg-induced cardiac vulnerability. Finally, the roles of RSS on the heart were examined. RSS decreased after myocardial ischemia reperfusion (I/R) injury. Moreover, in the mouse hearts after I/R, CARS2 mRNA expression decreased. Then, CARS2 heterozygous-deleted (*Cars2*[(+/-)]) mice were used to examine whether CARS2 affect cardiac robustness. *Cars2*[(+/-)] mice were vulnerable to I/R while there were no significant differences in cardiac and mitochondrial function under physiological condition. This

vulnerability of *Cars2*[(+/-)] mice might be due to mitochondrial dysfunction because CARS2 knockdown in cardiomyocytes induced decrease in mitochondrial membrane potential under hypoxic condition. Not only RSS synthesis but also RSS catabolism might contribute to the development of I/R-induced heart failure. Overall, this study suggests that RSS metabolism can be important for mitochondrial homeostasis and cardiac robustness, indicating new insight for redox biology.

Materials and Methods

Animals

All animal experiments were reviewed and approved by the ethics committees at the National Institutes of Natural Sciences. C57BL/6J mice were purchased from Japan SLC and Charles River Laboratories Japan. *Cars2*[(+/-)] mice were provided by Prof. T. Akaike (Tohoku University). Genotyping of *Cars2*[(+/-)] mice were conducted with mouse-tail DNA by polymerase chain reaction using PrimeSTAR GXL DNA Polymerase (Takara Bio). Sprague-Dawley (SD) rats were from Japan SLC. All animals were maintained under air-conditioned and 12 hours light/dark cycle.

MI surgery and cilnidipine treatment

Six weeks old C57BL/6J mice were anesthetized by isoflurane (Abbvie), and intubated and ventilated. Then, chest cavity was open at the intercostal space. Left anterior descending artery was ligated, and then chest cavity was closed. At the end of the surgery, buprenorphine was intraperitoneally injected as an analgesic. Cilnidipine (20 or 30 mg/kg/day) or saline (vehicle) was administered by a mini-osmotic pump (ALZET) one week or one day after the MI surgery.

Transmission electron microscopy and analysis of mitochondrial morphology

Mouse hearts were harvested and washed in ice cold phosphate-buffered saline (PBS). Then, hearts were fixed and processed for transmission electron microscopy imaging as described previously[11]. Imaging was performed using JEOL1010 microscope

(JEOL) with a Veleta CCD camera (Olympus). Mitochondrial circularity was calculated using ImageJ software (National Institutes of Health).

Pressure overload model, MeHg exposure and NaHS treatment

TAC surgery was performed as described previously[26]. Briefly, 6 weeks old C57BL/6J mice were anesthetized by isoflurane (Abbvie), and intubated and ventilated. Then, chest cavity was open at the intercostal space. Transverse aorta was constricted between the brachiocephalic artery and the left carotid artery by the width of 27-gauge needle. At the end of the surgery, buprenorphine was intraperitoneally injected as an analgesic. MeHg exposure was started 1 week before TAC surgery. MeHgCl (Sigma) was dissolved in drinking water (10 ppm) and mice were freely accessible. NaHS (Wako, 50 µmol/kg/day) or PBS (vehicle) was administered using mini-osmotic pump (ALZET) 3 days before TAC surgery.

Myocardial I/R surgery and intracardial sodium tetrasulfide injection

Two-three months old mice were anesthetized by isoflurane (Pfizer), and intubated and ventilated. Then, chest cavity was open at the intercostal space. Left anterior descending artery was ligated with PE10 polyethylene tube for 15 min to stop the blood flow (ischemia) and then, ligation was removed to restart the blood flow (reperfusion). After that, chest cavity was closed and buprenorphine was intraperitoneally injected as an analgesic. Sodium tetrasulfide (Na_2S_4, DOJINDO LABORATORIES) (3 nmol) was injected intracardially just after the ischemia.

TTC staining

Twenty-four hours after I/R, left anterior descending artery was re-ligated and 500 µL of 1% Evans Blue (Tokyo Chemical Industry) in PBS was perfused via inferior vena cava. Then, the heart was harvested, washed in ice cold PBS, and frozen in -30℃ for 2 hours. The frozen tissue was sliced in 1 mm thickness and immersed in 1% triphenyl tetrazolium chloride (TTC, Tokyo Chemical Industry) in PBS at 37℃ for 15 min. After that, the cardiac slices were immersed in 10% neutral-buffered formalin (Nacalai Tesque) at room temperature for 15 min. The stained slices were photographed and ischemic region was measured by ImageJ software.

Echocardiography

Chapter 1, 2

Echocardiography was performed by using Nemio-XG echocardiography (Toshiba) with a 14 MHz transducer, as described previously[26,27]. Mice were anesthetized by isoflurane (Abbvie) before echocardiography. Cardiac contractile function was measured by M-mode.

Chapter 3

Mice were anesthetized by isoflurane (Pfizer) and echocardiography was performed by using VEVO3100 with MX400 20-46 MHz transducer (Fujifilm VisualSonics). Cardiac contractile function was measured by 4D-mode and M-mode and analyzed by VevoLAB software (Fujifilm VisualSonics).

Analysis of mRNA expression

Total RNA were isolated from mouse hearts using RNeasy Fibrous Tissue Mini Kit (Qiagen) or from neonatal rat cardiomyocytes (NRCMs) using RNeasy Mini Kit (Qiagen) as previously described[28]. mRNA expression was analyzed by quantitative real-time PCR (qPCR) using Lightcycler 96 (Roche) with KAPA SYBR FAST qPCR kit (KAPA BIOSYSTEMS), as previously described[27]. The sequence of the primers used for qPCR were as follows: mouse CARS2 forward 5'-AAGCTGGTCAACACGGTTCC-3', reverse 5'-GCTTCCGAACACCTCACTGG-3'; mouse SQOR forward 5'-CTTCCCAAACACTCCGGTGA-3', reverse 5'-TGGGTCGCTTTCCAGTCTTC-3'; mouse ETHE1 forward 5'-TTGTCCTGAACGACCAGAGC-3', reverse 5'-GAAACTGTGAGCCCGTGGTA-3'; mouse SUOX forward 5'-AATTGTTCCGCTGCCGACAT-3', reverse 5'-AGGGGGTTGACTTGACTCTGA-3'; mouse TST forward 5'-GGAGCCGGATATAGTAGGACT-3', reverse 5'-AGCCATCGTAAACAGCCACA-3'; rodent 18S ribosomal RNA forward 5'-ATTAATCAAGAACGAAAGTCGGAGGT-3', reverse 5'-TTTAAGTTTCAGCTTTGCAACCATACT-3'; mouse CARS1 forward 5'-TGGTCAGTCAGTGCAACCTC-3', reverse 5'-GGCCCCAAAGATCTTCAGCA-3'; mouse 3-MST forward 5'-GCAGCTCGATCCCTCTTTCA-3', reverse 5'-CAGGTTCGATGCCATCTCGG-3'; rat CARS2 forward 5'-GGACGCAGTCTCCTGGTATAG-3', reverse 5'- ACTGGTCAGGATCCTTCGGA-3'.

RSS imaging in cardiac tissue

The mouse hearts were harvested and embedded in O.C.T. compound (Sakura Finetek), and frozen in cold isopentane to make fresh-frozen section. The section was sliced in 12 μm thickness. For SSip-1 DA imaging, 10 μM of SSip-1 DA (Goryo

Chemical) with 1 mg/mL bovine serum albumin (BSA, Nacalai Tesque) and 0.02% Cremophor (Sigma) was loaded at room temperature for 45 min. For QS10 imaging, 1 μM QS10 [provided from Dr. K. Umezawa (Tokyo Metropolitan Institute of Gerontology)] with 0.02% Pluronic F-127 (Invitrogen) was loaded at room temperature for 15 min. Then, section was mounted with ProLong Diamond Antifade Mountant with DAPI (Invitrogen). Imaging was performed using BZ-X700 microscope (KEYENCE).

Isolation of NRCMs and CARS2 knockdown by siRNA transfection

NRCMs were isolated from SD rats pups (1 to 2 days old) as described previously[26,29]. Isolated NRCMs were cultured in Dulbecco's Modified Eagle's Medium with low glucose (1 mg/mL) (D-MEM, Fujifilm Wako) containing 10% fetal bovine serum under 5% CO_2. To avoid proliferation of non-cardiomyocyte cells, 200 μM bromodeoxyuridine (Sigma) was used. For knockdown, Stealth siRNAs for CARS2 (#1, RSS323485; #2, RSS360017, Invitrogen) and Stealth RNAi™ siRNA Negative Control Med GC Duplex #3 (Invitrogen) for siControl were used. NRCMs were transfected with 20 nM siRNA using Lipofectamine RNAiMAX Transfection Reagent (Invitrogen) following manufacture's instruction.

RSS, hydrogen sulfide, and mitochondrial membrane potential imagings in NRCMs

Isolated NRCMs were plated on φ8 triple well glass base dish (Iwaki) coated with Matrigel (Corning). For RSS imaging, 1 μM QS10 was loaded with 0.02% Pluronic F-127 at 37°C for 15 min. For hydrogen sulfide (H_2S) imaging, 2.5 μM SF7-AM (Cayman Chemical) with 0.02% Cremophor was loaded at 37°C for 30 min. For mitochondrial membrane potential imaging, 1 μg/mL JC1 (Abcam) was loaded at 37°C for 30 min.

14

Imaging was performed using BZ-X700 microscope and analysis was performed using ImageJ software.

Isolation of adult mouse cardiomyocytes and mitochondrial membrane potential imaging

Isolation of adult mouse cardiomyocytes was performed as described previously[30]. Briefly, 2-3 months old mice were heparinized and then sacrificed by intraperitoneal injection of overdose of sodium pentobarbital. The heart was harvested and washed gently in ice cold cell isolation buffer (130 mM NaCl, 5.4 mM KCl, 25 mM HEPES, 0.33 mM NaH_2PO_4, 22 mM glucose, pH was adjusted in 7.4) supplemented with 0.5 mM $MgCl_2$, 50 μU/mL bovine insulin (Sigma) (CIB), and 0.4 mM EGTA (CIB + EGTA). Then, the aorta was clamped and the heart was perfused with CIB + EGTA. After that, perfusion with enzyme solution [1 mg/mL collagenase type II (Worthington), 0.06 mg/mL trypsin (Sigma), 0.06 mg/mL protease (Sigma), 0.3 mM $CaCl_2$, dissolved in CIB] was performed. After finishing digestion by enzymes, the heart was minced in enzyme solution supplemented with 0.2% BSA and 0.7 mM $CaCl_2$. Minced heart suspension was filtrated through 100 μm cell strainer (Falcon) and centrifuged for 3 min at 300 rpm. After supernatant was removed, the pellet was resuspended in CIB supplemented with 0.2% BSA and 1.2 mM $CaCl_2$, and incubated at 37°C for 10 min. The suspension was centrifuged again (3 min, 300 rpm), and supernatant was removed and the pellet was resuspended in Tyrode buffer (140 mM NaCl, 5.4 mM KCl, 5 mM HEPES, 0.33 mM NaH_2PO_4, 5.5 mM glucose, pH was adjusted in 7.4) supplemented with 1.8 mM $CaCl_2$, 0.5 mM $MgCl_2$, 0.2% BSA. Isolated cardiomyocytes were plated on φ12 glass base dish (Iwaki) coated with Matrigel and incubated at 32°C for 1.5 hr. For mitochondrial

membrane potential imaging, 1 µg/mL JC1 was loaded at 32°C for 30 min. Imaging was performed using BZ-X700 microscope and analysis was performed using ImageJ software.

Protein polysulfidation assay

Mouse hearts were homogenized and lysed in lysis buffer [40 mM phosphate (pH 7.4), 150 mM NaCl, 1% Triton X-100, 0.1% sodium dodecyl sulfate (SDS), 3 mM tyrosine, adjusted pH 7.4] with protease inhibitors (aprotinin and pepstatin A) and protein was extracted. After that, 100 µM EZ-Link Iodoacetyl-PEG2-Biotin (IAA-biotin, ThermoFisher Scientific) was added to protein sample and incubated at 37°C for 30 min. Excess IAA-biotin were removed using PD SpinTrap G-25 (Cytiva), and then Pierce™ Control Agarose Resin (ThermoFisher Scientific) was added to the samples and rotated at 4°C for 2 hours to remove proteins which binds to agarose. After centrifugation, Pierce™ High Capacity NeutrAvidin™ Agarose (ThermoFisher Scientific) was added to the supernatant and rotated at 4°C for 3 hours. The samples were centrifuged and resins were washed. The proteins which bind to NeutrAvidin Agarose were eluted by 15 min shaking in elution buffer [40 mM phosphate (pH 7.4), 150 mM NaCl, 1% Triton X-100, 0.1% SDS, 40 mM dithiothreitol (DTT)]. The eluted samples were separated by SDS-polyacrylamide gel electrophoresis (SDS-PAGE), and the proteins were stained by Flamingo Fluorescent Gel Stain (Bio-Rad). Imaging was performed using Typhoon FLA 9000 (GE Healthcare).

RNA-seq analysis

The heart was harvested from *Cars2*(+/+) and *Cars2*(+/-) mice and immediately frozen in liquified nitrogen. Whole cardiac tissue was homogenized in 1 mL of QIAzol Lysis Reagent (QIAGEN). Tissue homogenates were mixed with 200 µL of chloroform and centrifuged for 15 min at 12000 rpm, 4°C. Then, 600 µL of 70% ethanol was added to 600 µL of the supernatant and mixed. Total RNA in the mixture was isolated using RNeasy Mini Column (QIAGEN). RNA-seq analysis was performed and data were provided by Science Research Center (Yamaguchi University).

Statistical analysis

All results were shown as the means ± SEM acquired from at least 3 independent experiments. Statistical analysis was performed by unpaired t-test for comparison between two data sets or one-way analysis of variance (ANOVA) followed by Tukey's post hoc test for multiple comparison. The differences were considered to be significant when the values of $P<0.05$.

Results

Chapter 1. Cilnidipine improves heart failure after MI by suppressing mitochondrial hyperfission.

Because our group previously revealed that cilnidipine could inhibit mitochondrial hyperfission after hypoxic stress using neonatal rat cardiac fibroblasts[11], the effect of cilnidipine on mouse MI model were tested. MI surgery was performed 1 week before administration of cilnidipine and cardiac function was measured using echocardiography. Just before the drug administration, I confirmed that cardiac function was completely declined in MI mice (Figure 2A). Surprisingly, 3 weeks continuous administration of cilnidipine recovered cardiac function (Figure 2A, Table 2). I also revealed that treatment of cilnidipine improved mitochondrial fragmentation induced by MI (Figure 2B). These data suggest that mitochondrial quality control by cilnidipine is also effective *in vivo*.

Chapter 2. Restoration of Drp1 polysulfidation rescues MeHg-induced cardiac vulnerability to pressure overload.

In chapter 1, I found that mitochondrial quality control could be critical for cardiac robustness. Therefore, in this section, molecular details of mitochondrial quality control were focused. Our group reported that mitochondrial fission-inducing protein, Drp1, was critical for MI-induced cardiac senescence[11]. Moreover, cysteine residues of Drp1 are polysulfidated and depolysulfidation activates Drp1[12,20]. Furthermore, our group revealed that MeHg induced Drp1 depolysulfidation and caused cardiac vulnerability to pressure overload[12]. However, there are no therapeutic strategies for MeHg-induced cardiac vulnerability. Because sulfide donor NaHS reverses MeHg-induced Drp1 depolysulfidation[12], it was hypothesized that NaHS supplementation to MeHg-induced cardiac vulnerability mouse model were beneficial. After mice were exposed to MeHg for a week, cardiac pressure overload was induced by TAC surgery (Figure 3A). After TAC surgery, MeHg exposure was continued for another week and cardiac function was examined (Figure 3A). Prolonged exposure of MeHg along with TAC surgery caused significant decrease of cardiac contractility, indicating MeHg-induced cardiac vulnerability (Figure 3B, Table 3). In contrast, when NaHS was administered intraperitoneally for 10 days (from 3 days before TAC surgery to 7 days after TAC surgery, Figure 3A), the decrease in ejection fraction (EF, %) was significantly attenuated (Figure 3B, Table 3). These results suggest that the administration of sulfide donor is cardioprotective against MeHg-induced cardiac vulnerability.

Chapter 3. The role of RSS in cardiac robustness.

RSS in cardiac tissue were decreased after I/R injury.

In chapter 2, the physiological significance of Drp1 polysulfidation for cardiac robustness was demonstrated. The protein polysulfidation are mediated by several types of RSS via its high reactivity[21]. This high reactivity is thought to contribute to redox reaction in cells besides the protein polysulfidation. As mitochondria utilize series of redox reactions for ATP production (mitochondrial OXPHOS, Figure 1A), it was hypothesized that RSS could have important role for mitochondrial and cardiac homeostasis. Redox status of the cells within the heart tissue was changed by myocardial I/R injury, where blood and oxygen supply were temporarily stopped and mitochondrial OXPHOS was disrupted. After the reperfusion, recovery of blood flow in ischemic myocardial tissue causes generation of ROS[31], then changed myocardial redox status.

First, distribution of RSS in cardiac tissue under I/R injury was addressed. To visualize the distribution of RSS in cardiac tissue, fluorescent probe SSip-1 DA[32] was used. SSip-1 DA was loaded to fresh-frozen sections of the heart. The fluorescent signals from SSip-1 DA were decreased in I/R hearts, especially in ischemic region compared to non-ischemic region (Figure 4A), suggesting that ischemic stress induces decrease of RSS.

Next, molecular details of RSS decrease under hypoxic condition were examined. RSS can work as an electron acceptor and be reduced to H_2S[20,33]. Therefore, it was hypothesized that decrease of RSS induced by I/R was due to reduction of RSS. To test this, cellular RSS levels and H_2S levels were checked in cardiomyocytes under hypoxia. Molecular detection in NRCMs was achieved by fluorescent probes, QS10[34] for RSS and SF7-AM[35] for H_2S. After hypoxic stress, QS10 signals were decreased, indicating

decrease of RSS (Figure 4B). This data supports the results from *in vivo* experiments (Figure 4A). Moreover, SF7-AM signal was increased after hypoxic stress (Figure 4C), indicating that cellular H_2S levels were increased. These data suggest that intracellular RSS accept electrons and are reduced to H_2S under hypoxic condition.

Supplementation of RSS donor mitigated I/R-induced heart failure.

As decreased level of RSS was found in ischemic stress, it was hypothesized that supplementation of RSS could be protective for ischemic stress. To confirm it, I examined the effect of Na_2S_4, a common RSS donor, on the disease progression in I/R injury. Na_2S_4 was administered intracardially to I/R mice just after the ischemia procedure (Figure 5A). I confirmed that intracardial injection of Na_2S_4 increased RSS titer levels in cardiac tissues (Figure 5B). Moreover, Na_2S_4 injection mitigated cardiac dysfunction after I/R injury (Figure 5C), suggesting that RSS have protective effect against ischemic stress.

RSS-producing enzyme CARS2 expression was decreased in I/R hearts.

To further investigate the role of RSS on cardiac robustness, I asked whether endogenous RSS synthetic pathways are downregulated in response to ischemic stress. Previous report showed that CARS2 is main Cys-SSH synthase in mouse tissues and are thought to be critical for endogenous RSS production[20]. In addition, the protein expression of CBS and CSE, which are also known as RSS-producing enzyme, is limited in cardiac cells[25]. Therefore, I focused on CARS2 and mRNA expression of CARS2 in I/R-injured hearts was examined. In I/R model, left ventricle is more susceptible to the injury compared to other regions. Therefore, the hearts were divided into ischemic region (left ventricular wall) and non-ischemic region (right ventricular wall and interventricular

septum) (Figure 6A). Interestingly, the decrease of CARS2 expression was observed not only in the ischemic region but also in non-ischemic region (Figure 6B, C). These results imply that CARS2 expression can contribute to protection against ischemic stress and cardiac robustness.

$Cars2^{(+/-)}$ mice had normal cardiac geometry and mitochondrial function.

As CARS2 mRNA expression decreased in I/R hearts, I addressed whether CARS2 have important roles in cardiac robustness. Since $Cars2$-deficient ($Cars2^{(-/-)}$) mice are embryonic lethal[20], $Cars2^{(+/-)}$ mice were used to explore the physiological role of CARS2 in the cardiac robustness. Cardiac function and geometry of $Cars2^{(+/-)}$ mice were comparable to $Cars2^{(+/+)}$ mice (Figure 7A, B, Table 4). Moreover, mitochondrial membrane potential and cell size of cardiomyocytes isolated from $Cars2^{(+/-)}$ mice also had no significant differences to wild-type (WT) mice (Figure 7C). These results indicate that partial deficiency of CARS2 does not induce any phenotypical changes.

$Cars2^{(+/-)}$ mice were vulnerable to I/R injury.

As no apparent phenotypic differences were observed in $Cars2^{(+/-)}$ mice, the stress resistance of $Cars2^{(+/-)}$ mice against I/R injury was evaluated. In $Cars2^{(+/-)}$ mice, cardiac function after I/R was significantly decreased compared to $Cars2^{(+/+)}$ mice (Figure 8A, Table 5). Cardiac function of $Cars2^{(+/+)}$ mice gradually recovered after reperfusion, in which no significant difference was observed by day 7 post surgery compared to pre-operative day 0. In contrast, EF(%) of $Cars2^{(+/-)}$ mice dropped drastically 24 h after reperfusion, and remained at a low level over time compared to pre surgery, suggesting that these mice showed no recovery in cardiac function (Figure 8A). Moreover, TTC

staining revealed that *Cars2*$^{(+/-)}$ hearts showed significant increase of infarcted zone (Figure 8B). On the other hand, area at risk was not different between *Cars2*$^{(+/+)}$ and *Cars2*$^{(+/-)}$ hearts (Figure 8B), indicating that the extent of myocardium subjected to ischemic insult was comparable between two groups. RSS level in cardiac tissue was evaluated using fluorescent probe SSip-1 DA and QS10. In sham mice, both SSip-1 DA and QS10 signal intensity were similar between *Cars2*$^{(+/+)}$ and *Cars2*$^{(+/-)}$ hearts (Figure 8C). However, in the hearts from 15 min ischemia followed by 7 days reperfusion, both SSip-1 DA and QS10 signals were dramatically decreased in *Cars2*$^{(+/-)}$ compared to *Cars2*$^{(+/+)}$ mouse hearts (Figure 8C). These data suggest that CARS2 has critical role for protecting against ischemic stress, and that RSS synthesized by CARS2 are important for cardiac robustness.

CARS2 knockdown in NRCMs caused impairment of mitochondrial membrane potential after hypoxic stress.

To test whether CARS2 expression affect to mitochondrial functional integrity, mitochondrial membrane potential of CARS2 knockdown NRCMs was examined. For knockdown of CARS2, two different siRNAs (siCARS2 #1 and siCARS2 #2) were used. Both siRNAs successfully silenced the mRNA expression of CARS2 (Figure 9A). Under normoxic condition (21% O_2), mitochondrial membrane potential was comparable between negative control (siNC) and CARS2 knockdown (Figure 9B). However, under hypoxic condition (1% O_2), mitochondrial membrane potential in CARS2-silenced NRCMs were decreased compared to siNC (Figure 9C). These results indicate that CARS2 is essential for maintaining mitochondrial functional integrity in cardiomyocytes under hypoxic conditions.

Global protein polysulfidation did not change in CARS2 deficient mice.

Next, global protein polysulfidation in $Cars2^{(+/-)}$ mouse hearts was checked because Cys-SSH generated by CARS2 can be donor for protein polysulfidation[20,21]. To specifically detect the levels of global protein polysulfidation from $Cars2^{(+/+)}$ and $Cars2^{(+/-)}$ hearts, protein lysates underwent a series of chemical reactions (IAA-biotin trapping method) (Figure 10A). First, alkylating agent (IAA-biotin) attached to thiol groups (-SH) in proteins and this made all -SH biotinylated. Then, biotinylated (that means -SH containing) proteins were precipitated by avidin-conjugated beads. As polysulfidated thiol groups have electrophilicity, while -SH do not, polysulfidated proteins can be specifically eluted by reductant such as DTT (Figure 10A). Eluted polysulfidated proteins were separated and detected by SDS-PAGE. Several polysulfidated proteins were increased or decreased after I/R injury, however, no changes were found between $Cars2^{(+/+)}$ and $Cars2^{(+/-)}$ hearts (Figure 10B).

Changes in mRNA expressions of RSS catabolizing enzymes in I/R hearts.

RSS are known to be oxidized in mitochondria by several enzymes to avoid accumulation of H_2S and excess RSS[36] (Figure 11A). The mRNA expression levels of RSS catabolizing enzymes including sulfide:quinone oxidoreductase (SQOR), persulfide dioxygenase (ETHE1), sulfite oxidase (SUOX), and thiosulfate sulfurtransferase (TST) in I/R hearts were decreased in I/R hearts (Figure 11B-E), suggesting the compensation against reduction of RSS production through CARS2, to maintain endogenous RSS amounts in the heart.

CARS2 expression could be compensated by CARS1 in I/R-injured hearts.

CARS2 expression was downregulated in I/R-injured hearts (Figure 6). Previous reports have demonstrated that several enzymes, including CARS1[20], CBS[24], CSE[24], and 3-mercaptopyruvate sulfurtransferase (3-MST)[37] work as RSS-producing enzymes. Therefore, I hypothesized that the overall RSS-producing activity in I/R-injured hearts might be compensated by the upregulation of these RSS-producing enzymes. Under physiological condition, RNA-seq analysis revealed that there were no differences in mRNA expression levels of RSS-producing enzymes (CARS1, CBS, CSE, 3-MST) and catabolizing enzymes (SQOR, ETHE1, TST, SUOX) between $Cars2^{(+/+)}$ and $Cars2^{(+/-)}$ mouse hearts (Figure 12A). This result indicates that reduction in CARS2 expression was not compensated by other RSS-producing enzymes under physiological status. The expression levels of CBS and CSE were very low (Figure 12A) and undetected by qPCR. In contrast, CARS1 expression level was increased but 3-MST expression level was decreased in I/R-injured hearts (Figure 12B, 12C). As CARS1 is the only RSS-producing enzyme that was increased in I/R-injured heart, this result suggests that compensative CARS1 upregulation is critical for the maintenance of RSS production in I/R-injured hearts.

Discussion

Control of mitochondrial quality can be new therapeutic target for heart failure.

In the first part of this study, the effects of mitochondrial dynamics control by cilnidipine on MI-induced heart failure were examined. Cilnidipine improved cardiac contractile dysfunction and mitochondrial fragmentation after MI (Figure 2). Our previous study also revealed that cilnidipine inhibited cellular senescence in cardiomyocytes[11]. Therefore, this study suggests that mitochondrial quality control is critical for cardiac stress resistance. The recovery of cardiac function after the establishment of MI is remarkable because adult mammalian cardiomyocytes have poor regenerative capacity and have been considered not to recover cardiac function after injury[38]. In MI hearts, three regions were observed, infarct region, border zone, and remote region[39]. In infarct region, because dead cardiomyocytes are replaced by collagen fiber (scar), it is thought that there are few contributions to the recovery in cardiac function. Therefore, cilnidipine can be thought to have greater effect on cardiomyocytes located in border zone and/or remote region to improve cardiac dysfunction after MI. Indeed, in border zone, cardiomyocytes show senescent phenotype accompanied by mitochondrial fragmentation[11], and present study showed that cilnidipine attenuated MI-induced mitochondrial fragmentation (Figure 2B).

The molecular details of control of mitochondrial dynamics by cilnidipine.

Cilnidipine is one of the dihydropyridine calcium channel blockers, approved as an anti-hypertensive drug. However, several studies have indicated that cilnidipine may have additional effects besides lowering blood pressure[40]. Indeed, cilnidipine treatment

suppresses myocardial I/R injury in rabbits[41]. Recently, our group showed that control of mitochondrial dynamics by cilnidipine could be independent of calcium channel inhibition and cilnidipine can disrupt protein-protein interaction between Drp1 and filamin A (FLNa), an actin-binding protein[11]. Drp1-FLNa interaction is required for Drp1 activation and mitochondrial fission induced by hypoxic stress[11]. As Drp1 and FLNa are ubiquitously expressed[42,43] and related to many diseases including not only heart failure[11] but also Alzheimer's Disease[44,45], cilnidipine may be applicable for various therapeutics.

MeHg-induced cardiac vulnerability and modulation of Drp1 polysulfidation.

Drp1 is a redox-sensitive protein, and the cysteine residue can be modified by redox reaction and that induces changes in Drp1 activity[15,16]. As MeHg has high affinity to sulfhydryl group[17], cysteine residue can be a critical target for MeHg. Our previous study revealed that cysteine residues of Drp1 were polysulfidated and depolysulfidation by MeHg activated Drp1, which triggered mitochondrial hyperfission and cardiac vulnerability to pressure overload[12]. Moreover, sulfide donor NaHS recovers polysulfidation of Drp1[12]. Therefore, it was hypothesized that restoration of Drp1 polysulfidation rescues MeHg-induced cardiac vulnerability to pressure overload. Present study revealed that MeHg-induced cardiac vulnerability was mitigated by NaHS (Figure 3), suggesting that modulation of Drp1 polysulfidation is important for cardiac stress resistance.

MeHg is well-known as an environmental electrophile that causes neurotoxicity such as Minamata diseases[18]. MeHg can interact with cysteine amino acid and since MeHg adduct is similar to methionine, it enables transport of MeHg across the blood brain barrier through L-type neutral amino acid carrier transport system, leading to high

accumulation of MeHg in the brain[46,47]. Accumulated MeHg induces decrease in glutathione and glutamate dysregulation, causing neurotoxicity[46]. However, molecular mechanism and treatment for cardiotoxicity have not been elucidated. The present study shows that the regulation of protein polysulfidation determines prognosis of MeHg-induced cardiac vulnerability to pressure overload and is a potential therapeutic strategy for MeHg-induced cardiac vulnerability. As the molecular mechanism for development of neurotoxicity and cardiac vulnerability induced by MeHg are totally different, it is unlikely that the protein polysulfidation strategy is beneficial for MeHg-induced neurotoxicity.

Not only environmental electrophiles but also endogenous electrophiles contribute to redox regulation. Previously, nitric oxide (NO)-dependent production of 8-nitroguanosine 3'5'-cyclic monophosphate (8-nitro-cGMP) were identified in cultured cells[48,49]. 8-nitro-cGMP reacts with sulfhydryl group in glutathione and cysteine residues of protein, referred as S-guanylation, thus 8-nitro-cGMP is proved to be electrophilic and redox-active[49]. Redox modification of Kelch-like ECH-associated protein 1 (Keap1) by S-guanylation activates downstream signaling pathways[48]. These reports and this study suggest that redox modification of proteins by electrophiles is universal and critical for cellular homeostasis. Interestingly, S-guanylation of proteins are inhibited by bacterial-derived RSS (persulfides)[50], suggesting functional interaction between redox modification and RSS. Considering this relationship may be important for cellular redox biology.

RSS contributed to myocardial ischemic stress resistance.

The result shown in chapter 2 suggests that the protein polysulfidation are important for cardiac robustness. The protein polysulfidation is mediated by small molecule polysulfides and persulfides[21], which are referred to as RSS. As RSS are highly redox-active (Table 1), it was hypothesized that RSS have important roles in the heart homeostasis besides the protein polysulfidation, because the heart is also redox-active organ. Therefore, I focused on the role of RSS in cardiac pathophysiology. I found that RSS were decreased after ischemic stress in cardiac tissue and reduced to H_2S in cardiomyocytes under hypoxic condition (Figure 4). Supplementation of RSS donor (Na_2S_4) alleviated I/R-induced heart failure (Figure 5), indicating that RSS are protective against myocardial ischemic stress. Also, these results suggest that reduction of RSS during ischemia is critical for ischemic stress resistance. The molecular mechanisms of RSS reduction within the cardiomyocytes remain unknown, but electron acceptance at mitochondrial electron transport chain (ETC) can be possible mechanism. It is known that some RSS are electrophilic[23], and are postulated to act as alternative electron acceptors along with O_2 in mitochondrial ETC. Under physiological condition, electrons from ETC are accepted by oxygen and generate H_2O[3] (Figure 1A). Under hypoxic condition, however, oxygen supply is deprived and becomes insufficient as an electron acceptor. In this situation, it is thought that RSS can be substituted for oxygen and maintain mitochondrial respiration. Indeed, in HEK293T cells, RSS are reduced in ETC-dependent manner[20]. Moreover, anaerobic organism can reduce RSS to generate ATP[51]. These observations imply existence of sulfur respiration in mammalian cells, which facilitates the flux of electrons in ETC involving classical oxygen respiration.

RSS may also contribute to mitigate oxidative stress. During ischemic stress induced by I/R injury, ROS are generated and cause oxidative stress[31]. One of the RSS,

glutathione persulfides are proved to have higher H_2O_2-scavenging activity than glutathione[24], suggesting that RSS protect cells from oxidative stress. Further analysis is needed to elucidate the antioxidative capacity of RSS in I/R-injured hearts.

Generation of RSS by CARS2 might be critical for ischemic stress resistance.

I found that mRNA level of CARS2, one of the RSS-producing enzymes, was decreased in I/R hearts (Figure 6). $Cars2^{(+/-)}$ mice were vulnerable to I/R injury (Figure 8A, 8B), and RSS levels were decreased in $Cars2^{(+/-)}$ I/R-injured hearts (Figure 8C). CARS2 knockdown in NRCMs decreased mitochondrial membrane potential under hypoxic condition (Figure 9), suggesting that RSS production by CARS2 could contribute to ischemic stress resistance via maintaining mitochondrial functional integrity.

CARS2 has been classically known as cysteinyl tRNA synthetase localized in mitochondria. That means, CARS2 is a dual functional protein: cysteinyl tRNA synthetase and Cys-SSH (RSS)-producing enzyme. Recent studies have shown that each catalytic center responsible for these two functions were spatially segregated, Cys78/257 being essential for cysteinyl tRNA synthetase activity, whereas Lys124/127/317/320 being critical for Cys-SSH (RSS)-producing activity in human CARS2[20]. Indeed, the mutation in cysteine residues of CARS2 causes attenuated protein translation and unchanged Cys-SSH formation, while mutation in lysine residues induces normal protein translation and decreased Cys-SSH formation[20]. For further analysis using these mutants are needed to show physiological significance of CARS2 as RSS-producing enzyme.

An extensive study seeking the methods to detect RSS in biological samples have been conducted. However, specific detection and quantification of RSS are still difficult because RSS are highly reactive and various types of RSS are produced in biological

systems. Indeed, reactive sulfur atom (sulfane sulfur) in RSS can easily transfer to other sulfur atoms[21,52], making it difficult to chase specific RSS. Moreover, various RSS are produced in biological systems including low molecular cysteine polysulfide (Cys-SS_nH), glutathione polysulfide (GSS_nH)[24] and large molecular protein polysulfide (protein-SS_nH)[20]. Recently, another active sulfur species were identified, whose molecular weight was larger than low molecular polysulfides but smaller than protein polysulfides[53]. To circumvent these difficulties in specific detection of RSS, I used fluorescent imaging to detect RSS in cardiac tissues for the first time. This method was useful for understanding global dynamics of RSS during ischemic stress. Technical progress is needed to confirm which types of RSS contribute to ischemic stress resistance.

RSS catabolism and cellular/tissue homeostasis

Sulfide and RSS are metabolized in mitochondria[36], that can make sulfide flux in cells. RSS can release H_2S by its reduction, and H_2S can be oxidized back to RSS by SQOR[36,54]. RSS are further oxidized by several enzymes such as ETHE1, TST, and SUOX[36,54]. Oxidized RSS can be excreted as thiosulfate and sulfate in serum and urine at high concentration[36]. This RSS-catabolizing pathway has been shown to be related to pathophysiology. For example, loss-of-function mutation of SQOR in brain, liver, and heart increases the sensitivity to hypoxic stress[54]. ETHE1 deficiency causes accumulation of thiosulfate and sulfide in mouse tissues including brain, liver, and muscle, exhibiting features of ethylmalonic encephalopathy[55]. Mutation in SUOX causes isolated sulfide oxidase deficiency, an autosomal recessive disorder[56,57]. TST mRNA and protein expression are correlated with fat mass and blood glucose in mouse adipose tissue and TST overexpression in mouse adipocyte is protective against high fat diet-induced obesity

via maintaining glucose and lipid homeostasis[58]. TST-deleted mice show impaired glucose and lipid homeostasis[58,59]. Taken together, these reports indicate that RSS and sulfide levels are strictly regulated, which is important for cellular/tissue homeostasis. However, the role of these enzymes in cardiovascular system is still unclear. This study experimentally demonstrated that SQOR, ETHE1, SUOX, and TST mRNA expression were decreased after I/R injury (Figure 11), suggesting a significant role of RSS catabolism in ischemic stress resistance. Further experiments are needed to elucidate physiological significance of RSS catabolism as well as RSS synthesis in cellular homeostasis.

RSS-producing enzymes in the heart.

Previous report has shown that bound sulfane sulfur (one form of RSS) was decreased in plasma from patients of cardiovascular diseases[60], implying biological significance of RSS in cardiovascular system. Previously, several enzymes have been identified as RSS-producing enzymes including CARS1/2[20], CBS[24], CSE[24], and 3-MST[37]. These RSS-producing enzymes are thought to be critical for cardiac robustness. Indeed, cardiac specific overexpression of CSE improves myocardial I/R-induced heart failure[61]. However, endogenous expression levels of CBS and CSE are barely detectable as described previously[25], which was confirmed by RNA-seq analysis (Figure 12A) in this study. Moreover, endogenous concentration of CysS-SCys (substrate for CBS and CSE for Cys-SSH production) is lower than that of Cys-SH (substrate for CARS2) (not detected and 13.3 µM, respectively)[24]. Furthermore, RSS production efficiency of CSE is also low compared to CARS2 (K_m value: 243.0 µM and 7.3 µM, respectively)[20], implying that neither CBS nor CSE contributes to RSS synthesis in the heart. 3-MST was the most

abundant RSS-producing enzyme in the heart (Figure 12A). However, RSS production efficacy of 3-MST is very low (K_m value: 4.5 mM of 3-mercaptopyruvate)[37]. Because 3-mercaptopyruvate (the substrate for 3-MST) is generated from Cys-SH[62], intracellular concentration of 3-mercaptopyruvate is considered to be similar or lower than that of Cys-SH. As the endogenous concentration of Cys-SH in the heart was revealed as 13.3 μM[24], it is thought that 3-MST cannot work as predominant RSS-producing enzyme in the heart. Indeed, 3-MST deficiency is protective against myocardial I/R injury[63], which is opposite to the results shown in most of other papers which showed that RSS are beneficial for cardiac robustness[12,60,61,64,65], including this study. Therefore, it is likely that CARS2 (or CARS1) is a principal RSS-producing enzyme in the heart.

RSS vs H$_2$S.

H$_2$S had been thought as important endogenous gasotransmitter[66] and extensive studies have shown that H$_2$S is cardioprotective[67,68]. In these studies, NaHS and sodium sulfide (Na$_2$S) are used as H$_2$S donor. These H$_2$S donors are widely used to elucidate biological significances of H$_2$S. However, whether these H$_2$S donor increase H$_2$S level in the heart were not checked in individual studies[67,68]. One study has shown that exogenous supplementation of Na$_2$S to tissue (liver and heart) homogenates fails to increase H$_2$S level and is absorbed into tissue as bound sulfur (one type of RSS)[69]. Indeed, our group has shown that NaHS treatment increases protein polysulfidation[12]. These results imply that RSS, but not H$_2$S, may predominantly mediate the protection of the heart against I/R injury. This study also showed that RSS were reduced to H$_2$S under hypoxic condition (Figure 4), suggesting the significance of sulfide catabolism in cardiac ischemic stress resistance.

Compartmentalization of RSS

As CARS2 and RSS catabolizing enzymes (SQOR, ETHE1, TST, SUOX) are predominantly localized in mitochondria, it is thought that RSS formation and catabolism may mainly occur in mitochondria. However, proteins localized outside of mitochondria are also polysulfidated[21]. These facts raise two possibilities. One is that RSS are produced in mitochondria and transported to cytosolic compartment. Although no transporters for RSS are found, some transporters for sulfur containing molecules are identified from mitochondrial membrane fractions. For example, Atm1, one of the ATP-binding cassette transporters, permeates active sulfur species from mitochondria to cytosol for tRNA thiolation[53]. Recently, SLC25A39, a mitochondrial membrane carrier, was identified as glutathione transporter into mitochondria[70]. Further analysis for these transporters may help to solve RSS dynamics between the subcellular compartments. Another possibility is that production of RSS is compartmentalized. In the heart, several RSS-producing enzymes are expressed (Figure 12A), and their localization is separated (CARS2: mitochondria, CARS1 and 3-MST: cytosol). Therefore, it is possible that RSS in mitochondria are derived from CARS2 and cytosolic RSS are from CARS1 and/or 3-MST. This idea is supported by the result that global protein polysulfidation level was not changed by CARS2 heterozygous deficiency (Figure 10B). Moreover, as several proteins were polysulfidated in mouse hearts after I/R that was independent of CARS2 expression level (Figure 10B), other RSS-producing enzymes may compensate the level of protein polysulfidation. Indeed, CARS1 was significantly upregulated in mouse hearts after I/R (Figure 12B).

In conclusion, I revealed that RSS and its metabolism could contribute to mitochondrial quality control and cardiac stress resistance in rodent hearts. My findings will provide a novel regulatory mechanism of mitochondrial quality by RSS and a breakthrough therapy against chronic heart failure.

Figures and figure legends

A
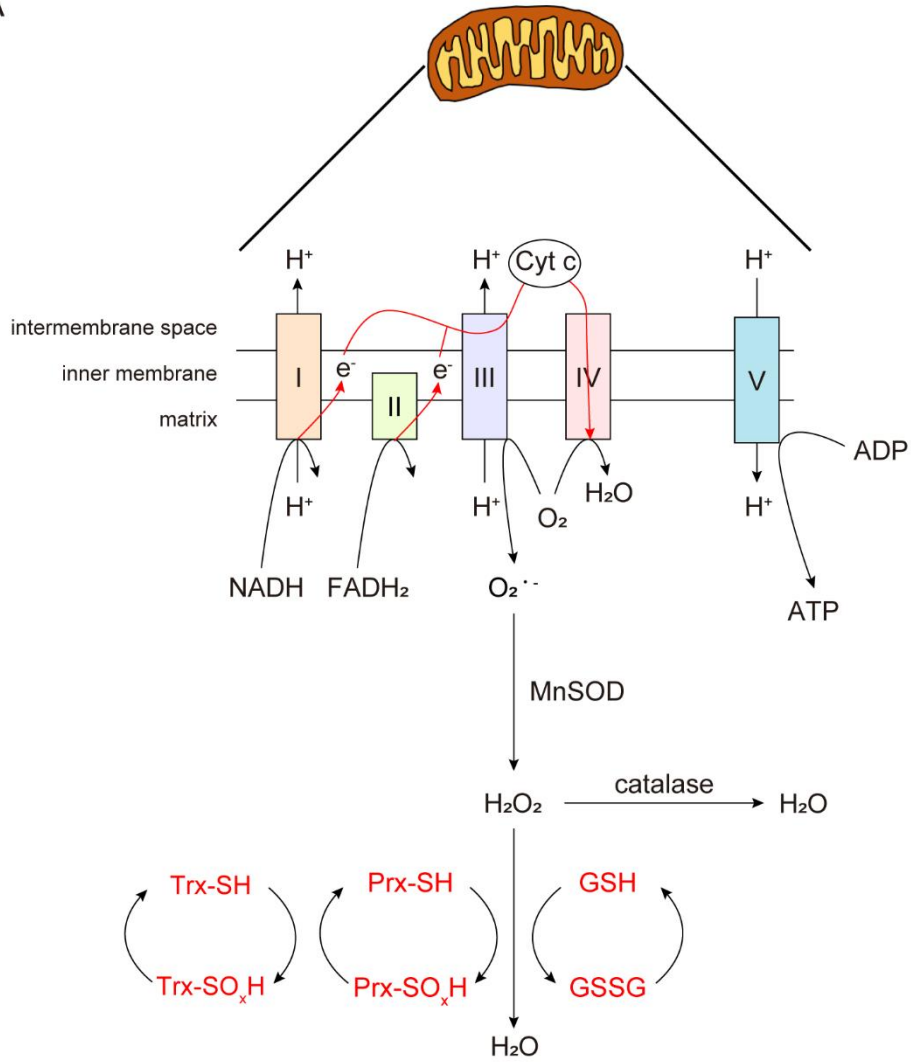
B
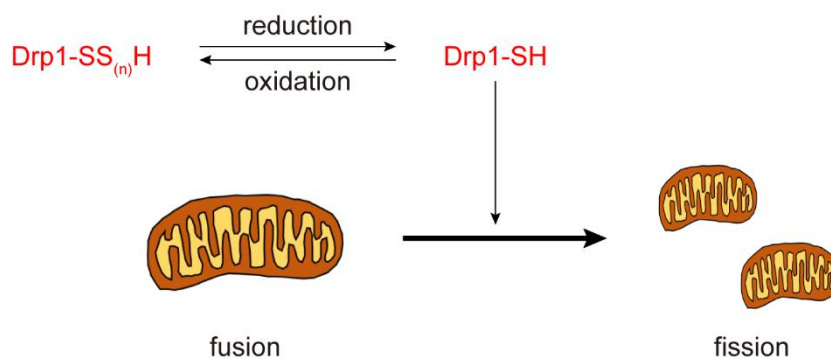
Figure 1. Redox signaling in mitochondrial respiration and quality control.

A. Schema of mitochondrial OXPHOS. Electrons are transported to generate proton gradient via redox reaction. ROS are also generated in OXPHOS system and reduced to H_2O by antioxidants, such as manganese superoxide dismutase (MnSOD)/catalase, glutathione (GSH, reduced form; GSSG, oxidized form), peroxiredoxin [Prx-SH, reduced form; Prx-SO_xH (x=1-2), oxidized form], and thioredoxin [Trx-SH, reduced form; Trx-SO_xH (x=1-2), oxidized form]. NADH, nicotinamide adenine dinucleotide; $FADH_2$, flavin adenine dinucleotide; I, NADH ubiquinone oxidoreductase (complex I); II, succinate dehydrogenase (complex II); III, ubiquinol-cytochrome c reductase (complex III); IV, cytochrome c oxidase (complex IV); V, ATP synthase (complex V); Cyt c, cytochrome c. Red arrows indicate the transportation of electrons. Red characters indicate cysteine-containing proteins that metabolize ROS. **B.** Schematic image of redox-dependent post-translational modification of Drp1 protein[12]. Reduction (=depolysulfidation) of Drp1 cysteine residue triggers Drp1 activation and mitochondrial hyperfission, leading to cardiac vulnerability to stress. Thus, redox-dependent control of Drp1 protein polysulfide is important for mitochondrial homeostasis.

A

B

sham vehicle
sham cilnidipine
MI vehicle
MI cilnidipine
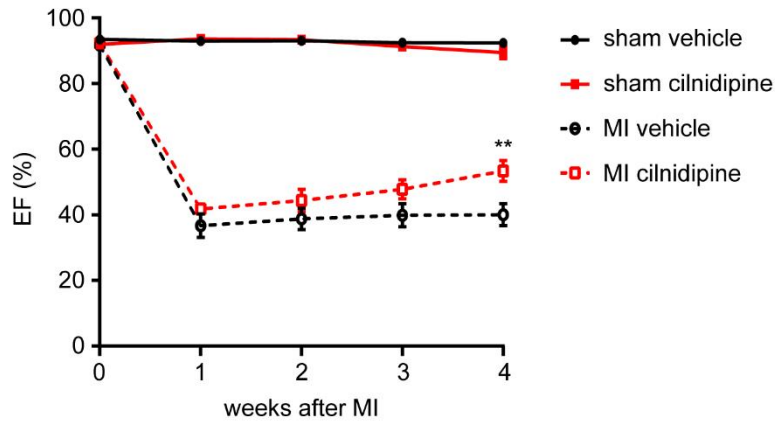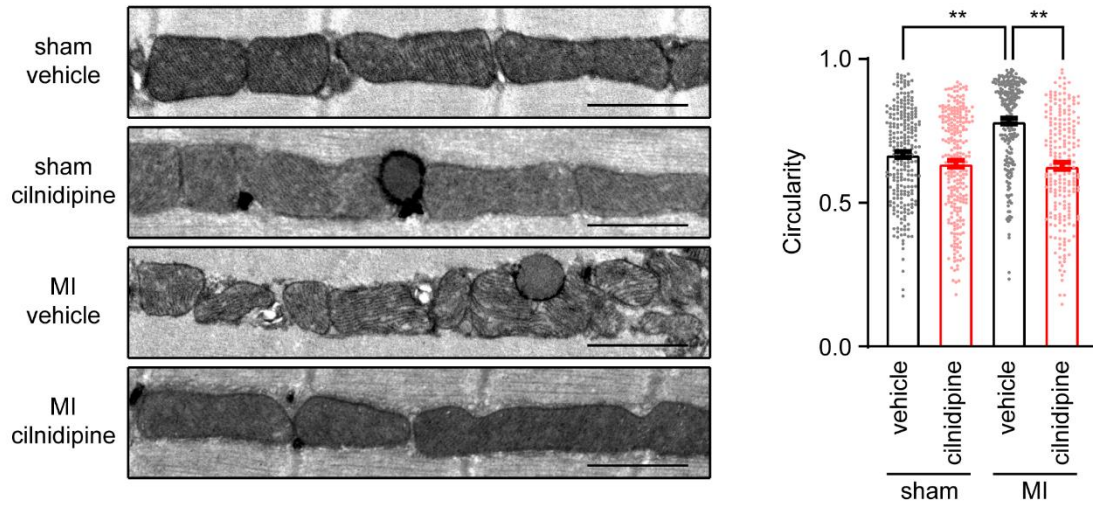
Figure 2. Treatment with cilnidipine 1 week after MI improves chronic heart failure.

A. Changes in left ventricular contractility (EF) before and after MI. Cilnidipine (20 mg/kg per day) was intraperitoneally administered at 1 week after MI. At week 0, sham vehicle n=3; sham cilnidipine n=5; MI vehicle n=4; MI cilnidipine n=6. At week 1-4, sham vehicle n=5; sham cilnidipine n=5; MI vehicle n=8; MI cilnidipine n=8. **B.** Cardiac mitochondrial morphology 1 week after MI. Cilnidipine (30 mg/kg per day) was intraperitoneally administered 1 day after MI. Sham vehicle, n=246 from 4 mice; sham cilnidipine, n=252 from 4 mice; MI vehicle, n=233 from 3 mice; MI cilnidipine, n=218 from 4 mice. Scale bars, 1 μm. Data are shown as the means ± SEM. [**]$P<0.01$ vs MI vehicle tested by one-way ANOVA (A). [**]$P<0.01$ tested by one-way ANOVA (B).

A

MeHg exposure
(10 ppm, dissolved in drinking water)

NaHS treatment
(50 μmol/kg/day, i.p.)

TAC
surgery

echocardiography

4 days   3 days   1 week
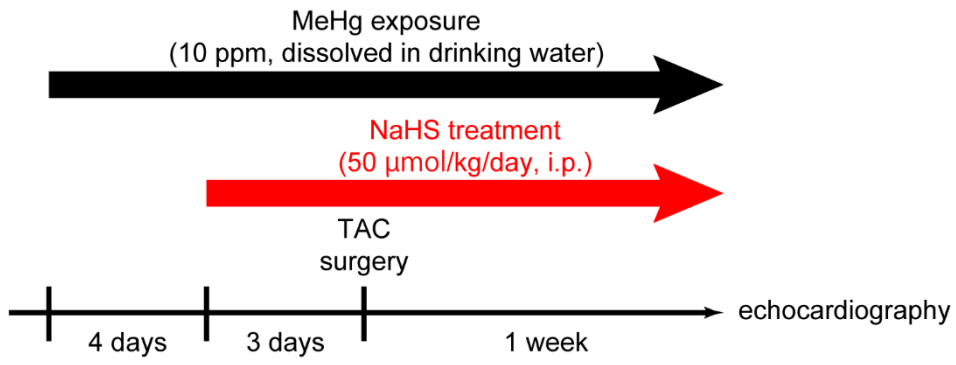
B
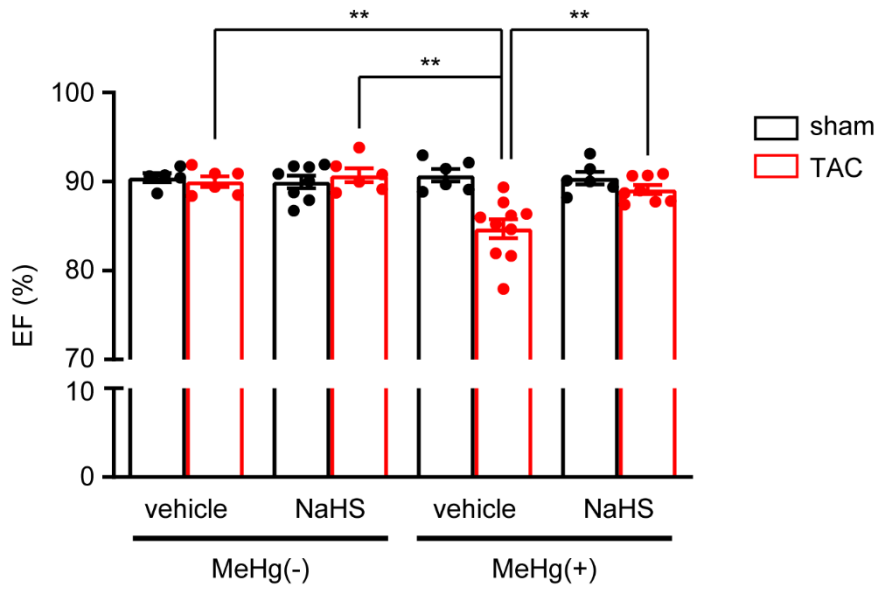
Figure 3. NaHS treatment prevents MeHg-induced cardiac vulnerability to pressure overload in mice.

A. Experimental protocol. **B.** Cardiac contractile function (EF) 1 week after TAC surgery was assessed using echocardiography. MeHg(-) vehicle sham n=5; MeHg(-) vehicle TAC n=6; MeHg(-) NaHS sham n=8; MeHg(-) NaHS TAC n=6; MeHg(+) vehicle sham n=6; MeHg(+) vehicle TAC n=10; MeHg(+) NaHS sham n=6; MeHg(+) NaHS TAC n=8. Data are shown as the means $\pm$ SEM. [**]$P<0.01$ tested by one-way ANOVA.
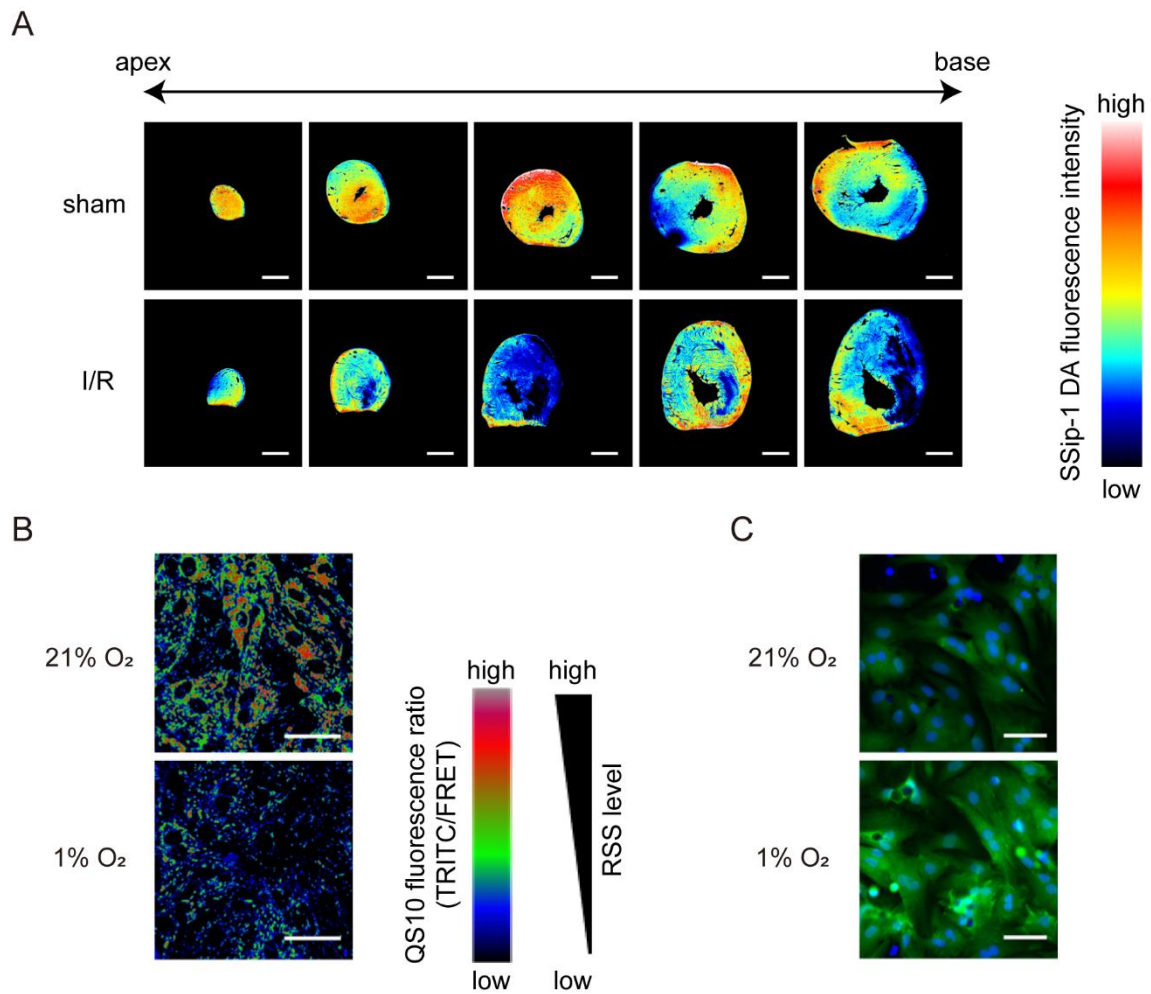
Figure 4. Decline of RSS level in mouse hearts after I/R injury and rat cardiomyocytes after hypoxic stress.

A. Visualization of RSS titers in mouse hearts after I/R injury using SSip-1 DA. Mice were exposed to 15 min ischemia followed by 24 hours reperfusion. Scale bars: 1 mm. **B.** RSS titers in NRCMs cultured under normal (21% O_2) or hypoxic (1% O_2) condition for 24 hours visualized by QS10. Scale bars: 40 μm **C.** H_2S titers in NRCMs visualized by SF7-AM. Scale bars: 50 μm.
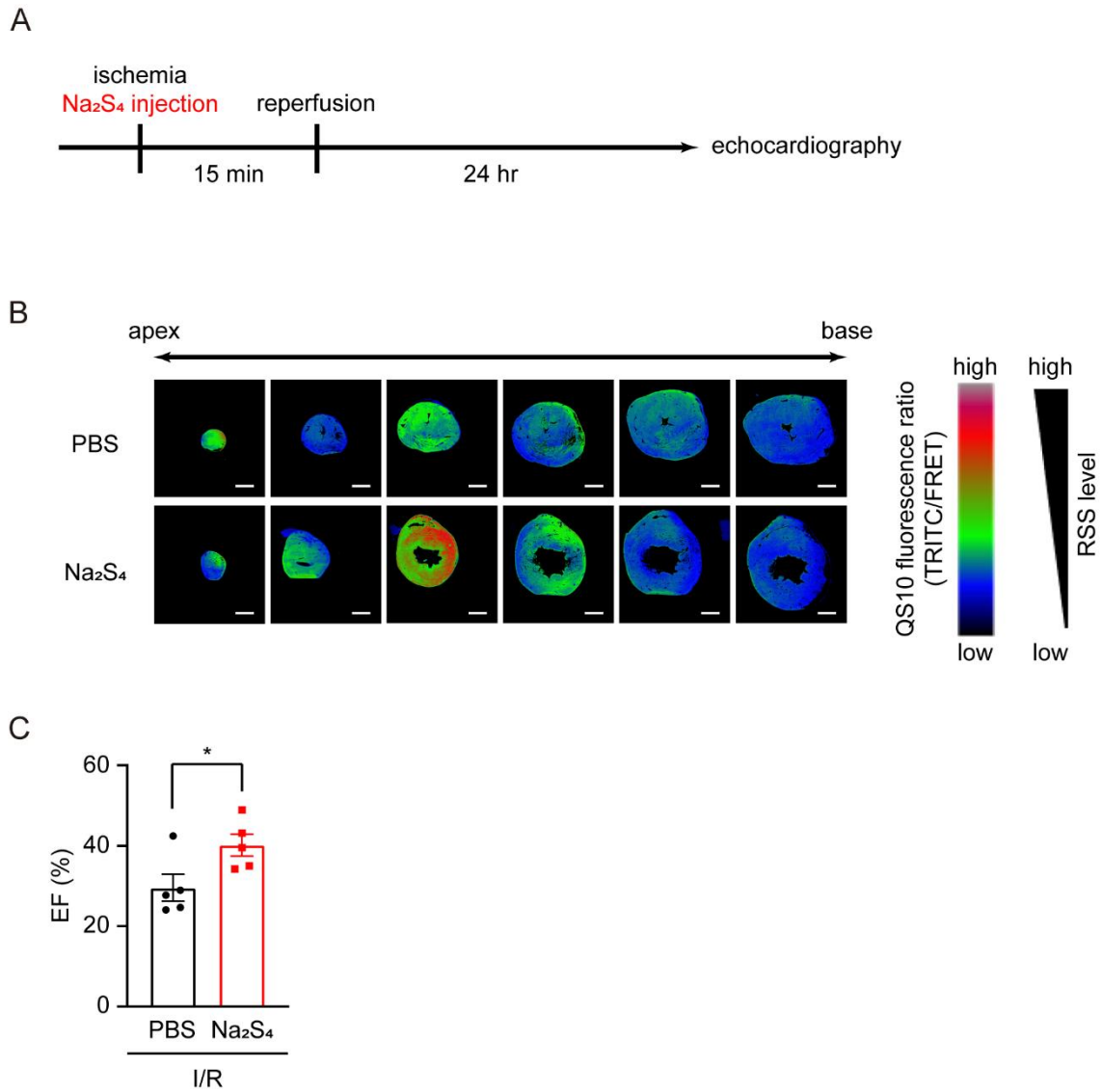
Figure 5. Intracardial injection of Na₂S₄ rescues I/R-induced heart failure.

A. Experimental protocol. **B.** RSS titers in Na_2S_4 (3 nmol)-injected ischemic cardiac tissue visualized by QS10. Scale bars, 1 mm. **C.** Cardiac contractile function (EF) after I/R. Mice were exposed to 15 min ischemia followed by 24 hours reperfusion. PBS n=5; Na_2S_4 n=5. Data are shown as the means ± SEM. [*]$P<0.05$ tested by t-test.
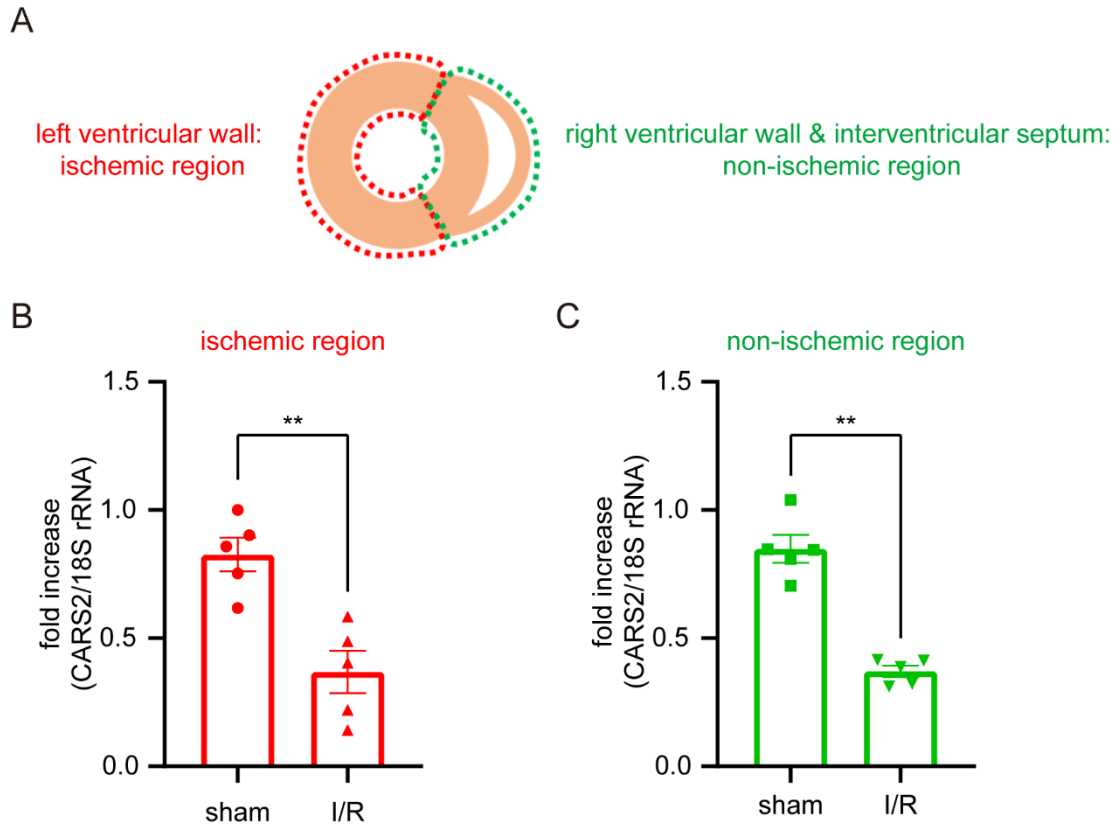
Figure 6. Decrease in CARS2 mRNA expression levels in mouse hearts after I/R.

A. Cardiac tissues were divided into ischemic region (left ventricular wall) and non-ischemic region (right ventricular wall and interventricular septum) for analysis of CARS2 mRNA expression. **B**, **C.** CARS2 mRNA expression levels in ischemic region (B) and non-ischemic region (C). Mice were exposed to 15 min ischemia followed by 24 hours reperfusion. Sham n=5; I/R n=5. Data are shown as the means $\pm$ SEM. [**]P<0.01 tested by t-test.
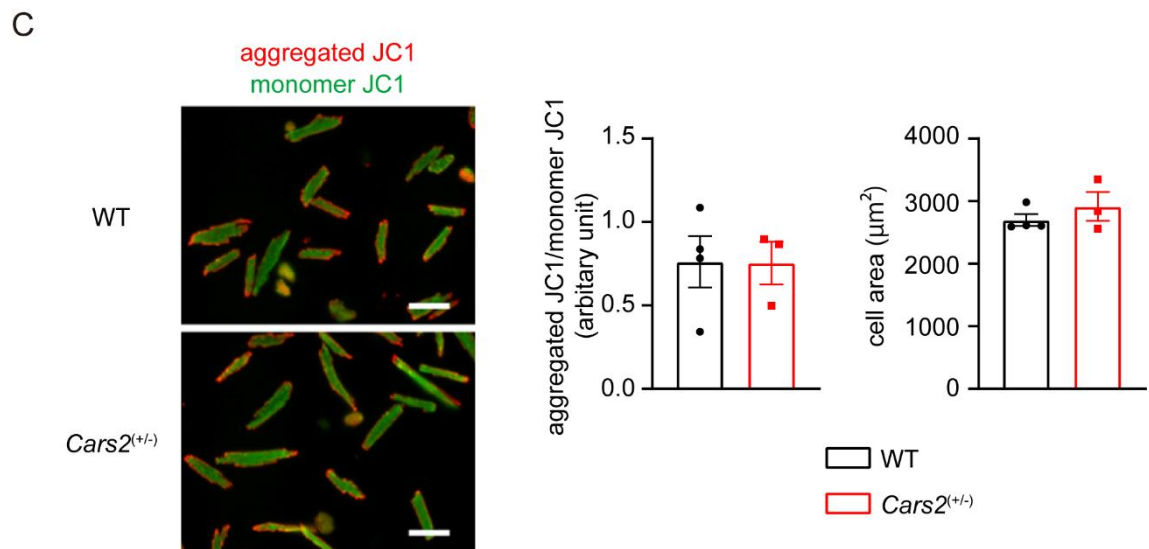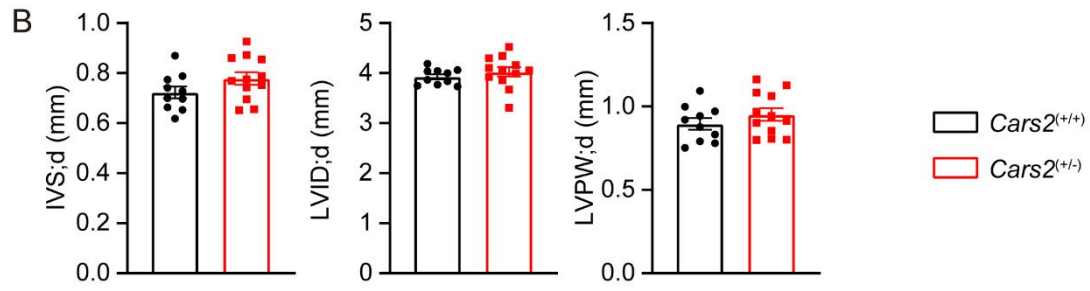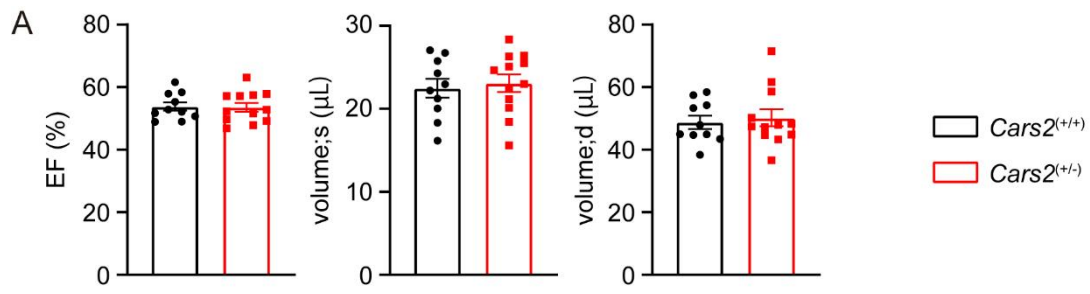
Figure 7. Cardiac contractility, geometry, and myocardial mitochondrial function of *Cars2*$^{(+/-)}$ mice.

A. Cardiac function of *Cars*2$^{(+/+)}$ and *Cars*2$^{(+/-)}$ mice measured by echocardiography. EF, left ventricular systolic volume (volume;s), and left ventricular diastolic volume (volume;d) were measured using 4D-mode analysis. **B.** Cardiac geometry of *Cars*2$^{(+/+)}$ and *Cars*2$^{(+/-)}$ mice measured by echocardiography. Interventricular septum thickness at diastole (IVS;d), left ventricular intra diameter at diastole (LVID;d), and left ventricular posterior wall thickness at diastole (LVPW;d) were measured using M-mode analysis. *Cars*2$^{(+/+)}$ n=10; *Cars*2$^{(+/-)}$ n=12. **C.** Mitochondrial membrane potential and cell area of cardiomyocytes isolated from WT and *Cars*2$^{(+/-)}$ mice were measured using JC1 staining. Red fluorescence means aggregated JC1, polarized mitochondria, and green fluorescence means monomer JC1, depolarized mitochondria. WT n=4; *Cars*2$^{(+/-)}$ n=3. Scale bars, 100 μm. Data are shown as the means ± SEM.

A

EF (%)

- Cars2(+/+) sham
- Cars2(+/+) I/R
- Cars2(+/-) sham
- Cars2(+/-) I/R

days after reperfusion

B

Cars2(+/+)

Cars2(+/-)

IZ/AAR (%)

AAR/total (%)

- Cars2(+/+)
- Cars2(+/-)

C

Cars2(+/+) sham   Cars2(+/-) sham   Cars2(+/+) I/R   Cars2(+/-) I/R

SSip-1 DA

QS10

1.8 RSS rich

QS10 TRITC/FRET

0.0 RSS poor

QS10 TRITC/FRET

sham

I/R
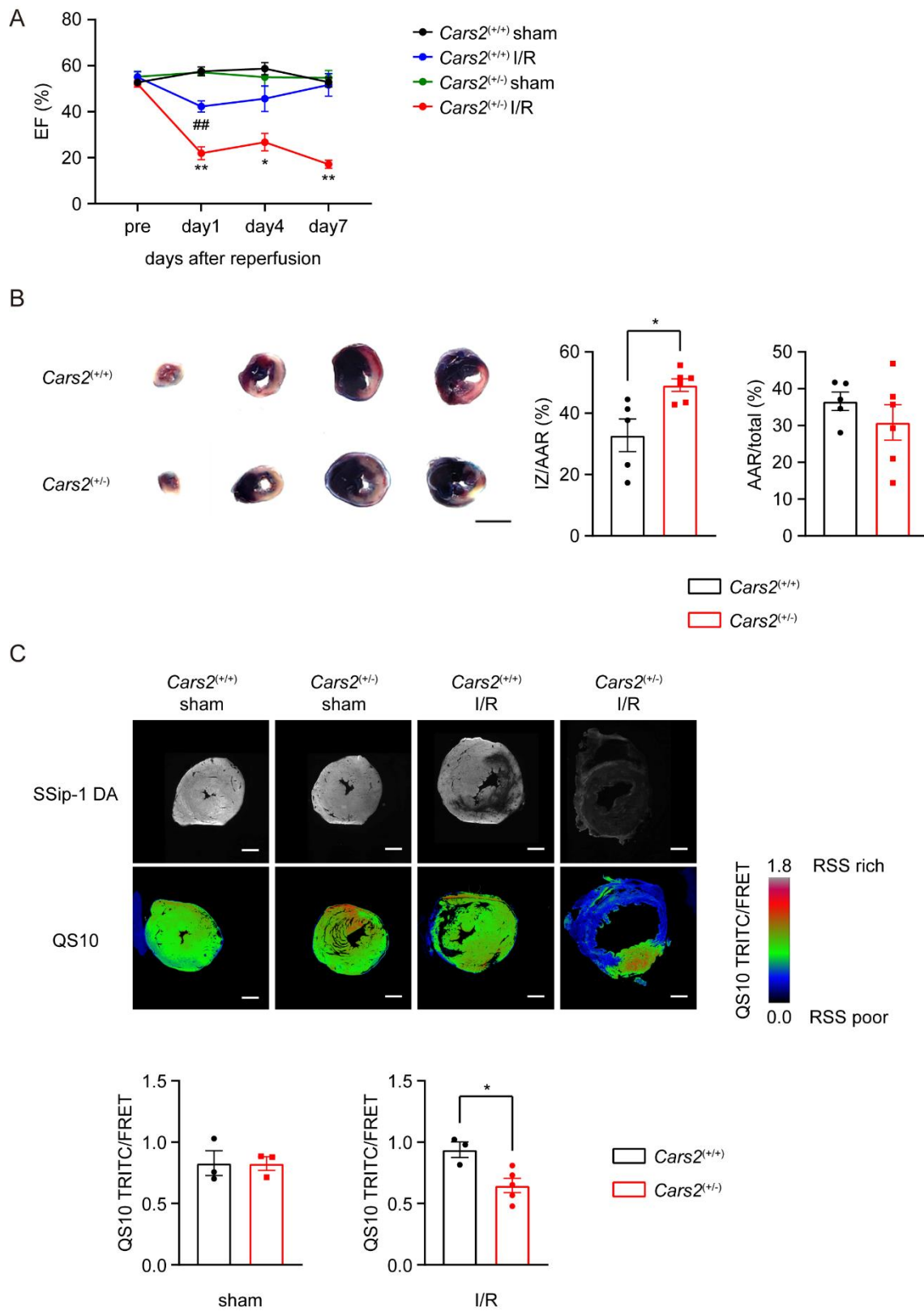
- Cars2(+/+)
- Cars2(+/-)

Figure 8. Exacerbation of cardiac I/R injury in *Cars*2$^{(+/-)}$ mice.

A. Cardiac function of *Cars*2$^{(+/+)}$ and *Cars*2$^{(+/-)}$ mice after I/R injury was measured by echocardiography. EF was measured using 4D-mode analysis. 15 min ischemia followed by reperfusion for indicated time was introduced. At pre, *Cars*2$^{(+/+)}$ sham n=5; *Cars*2$^{(+/+)}$ I/R n=5; *Cars*2$^{(+/-)}$ sham n=6; *Cars*2$^{(+/-)}$ I/R n=6. At day1, *Cars*2$^{(+/+)}$ sham n=4; *Cars*2$^{(+/+)}$ I/R n=4; *Cars*2$^{(+/-)}$ sham n=3; *Cars*2$^{(+/-)}$ I/R n=4. At day4, *Cars*2$^{(+/+)}$ sham n=5; *Cars*2$^{(+/+)}$ I/R n=5; *Cars*2$^{(+/-)}$ sham n=6; *Cars*2$^{(+/-)}$ I/R n=6. At day7, *Cars*2$^{(+/+)}$ sham n=5; *Cars*2$^{(+/+)}$ I/R n=5; *Cars*2$^{(+/-)}$ sham n=6; *Cars*2$^{(+/-)}$ I/R n=5. **B.** Representative images of TTC-stained cardiac slices from *Cars*2$^{(+/+)}$ and *Cars*2$^{(+/-)}$ mice after I/R injury. 15 min ischemia followed by 24 hours reperfusion was introduced. Infarcted zone (IZ), area at risk (AAR), and total area (total) were measured using ImageJ software. *Cars2*$^{(+/+)}$ n=5; *Cars2*$^{(+/-)}$ n=6. Scale bar, 3 mm. **C.** Representative images of RSS titers using fluorescent probes (SSip-1 DA and QS10) in *Cars*2$^{(+/+)}$ and *Cars*2$^{(+/-)}$ mice after I/R injury. 15 min ischemia followed by 1 week reperfusion was introduced. *Cars*2$^{(+/+)}$ sham n=3; *Cars*2$^{(+/-)}$ sham n=3; *Cars*2$^{(+/+)}$ I/R n=3; *Cars*2$^{(+/-)}$ I/R n=5. Scale bars, 1 mm. Data are shown as the means ± SEM. $^{*}P<0.05$, $^{**}P<0.01$ vs *Cars*2$^{(+/+)}$ I/R, $^{\#\#}P<0.01$ vs *Cars*2$^{(+/+)}$ sham tested by one-way ANOVA (A). $^{*}P<0.05$ tested by t-test (B, C).

A

B

aggregated JC1
monomer JC1

21% O₂

siNC

siCARS2 #1

siCARS2 #2

C

aggregated JC1
monomer JC1

1% O₂

siNC
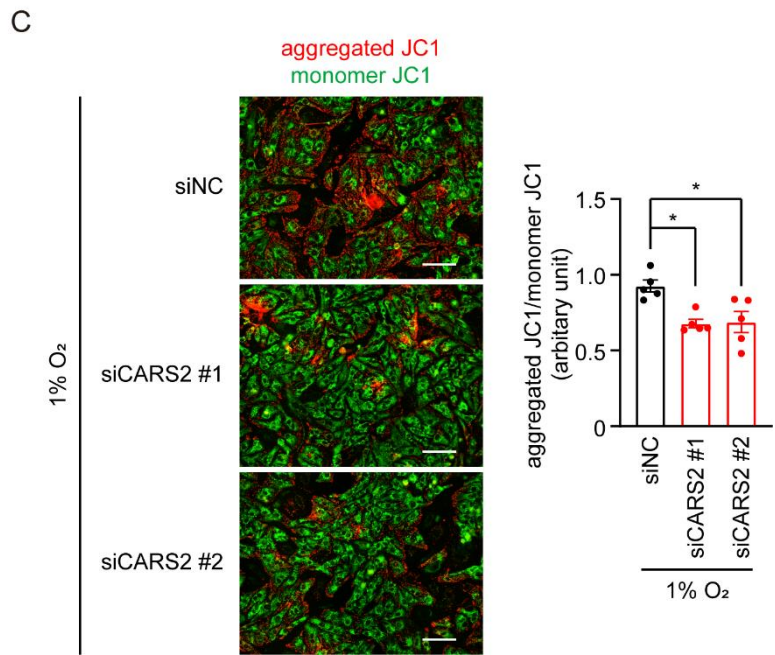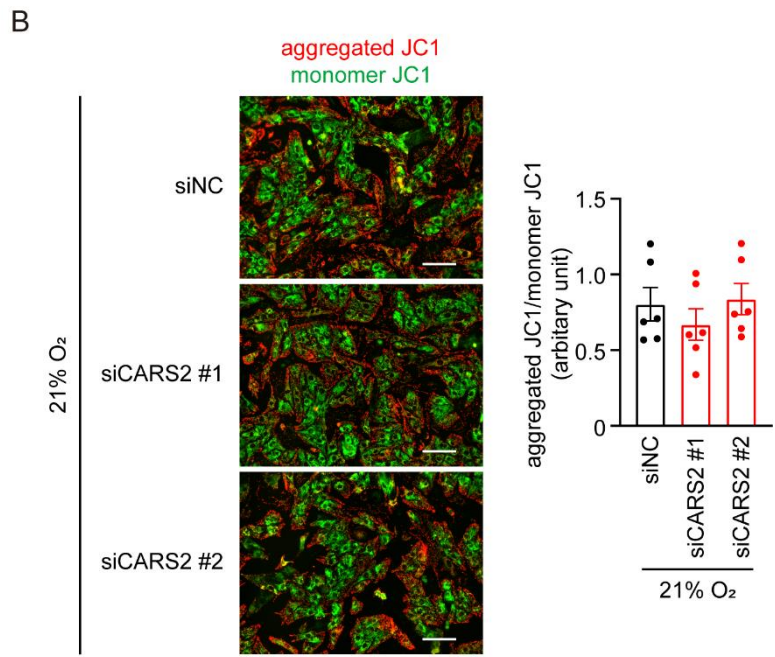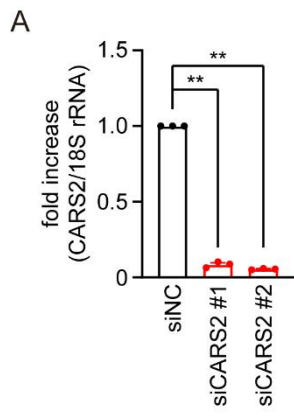
siCARS2 #1

siCARS2 #2

Figure 9. Reduction of mitochondrial membrane potential by CARS2 knockdown in NRCMs after hypoxic stress.

A. CARS2 mRNA expression in CARS2 knocked-down NRCMs. siNC, n=3; siCARS2 #1, n=3; siCARS2 #2, n=3. **B, C.** Mitochondrial membrane potential of CARS2 knocked-down NRCMs were examined by JC1 staining under 21% O_2 (B) and 1% O_2 (C) for 6 hours. Scale bars, 100 μm. In **B**, siNC, n=6; siCARS2 #1, n=6; siCARS2 #2, n=6 from three independent NRCMs isolation. In **C**, siNC, n=5; siCARS2 #1, n=5; siCARS2 #2, n=5 from three independent NRCMs isolation. Data are shown as the means ± SEM. [*]$P<0.05$, [**]$P<0.01$ tested by one-way ANOVA.

A

biotin—$\underset{H}{N}$—...—$\underset{H}{N}$—$\overset{O}{C}$—I

IAA-biotin

precipitated by avidin-conjugated beads

DTT (electrophiles)

eluted

B

	input								elution							
	Cars2(+/+)				Cars2(+/−)				Cars2(+/+)				Cars2(+/−)			
I/R	−	−	+	+	−	−	+	+	−	−	+	+	−	−	+	+

short exposure

long exposure
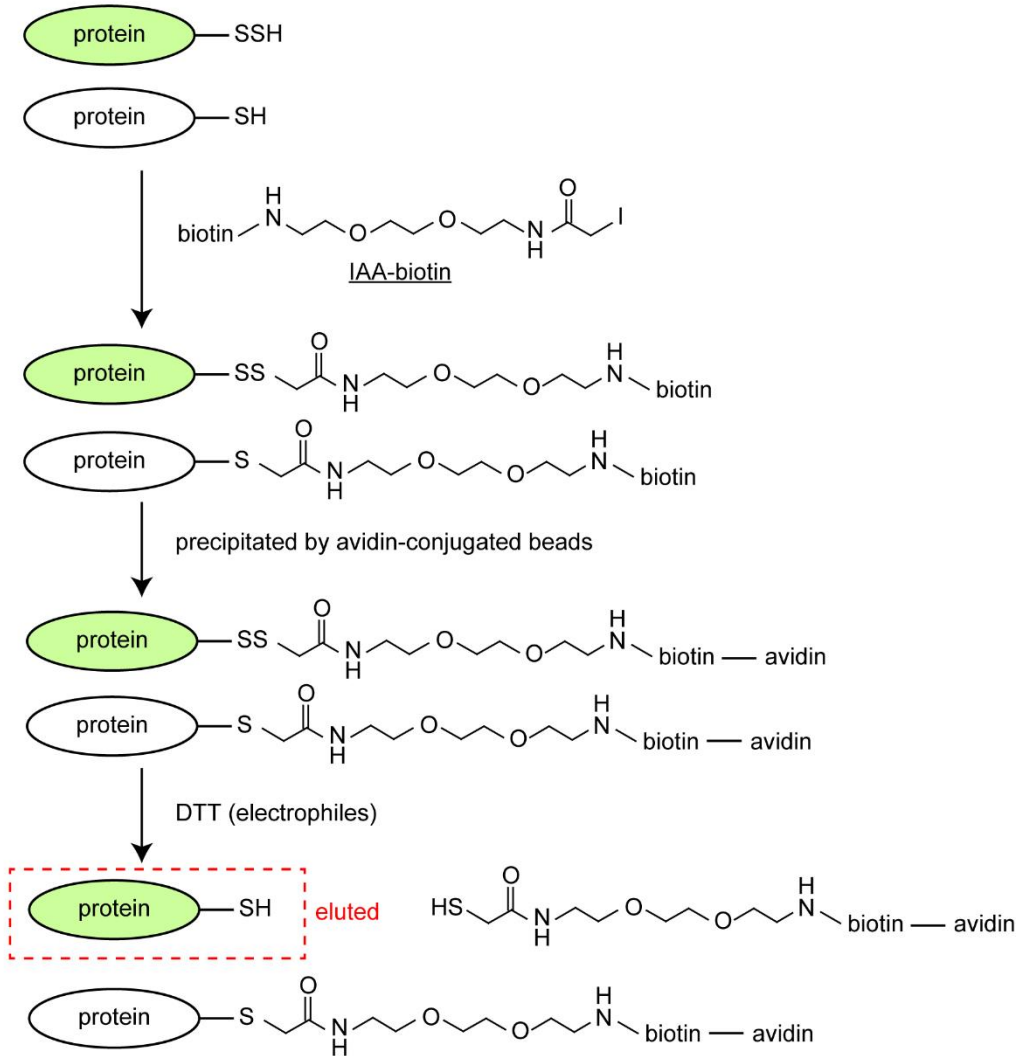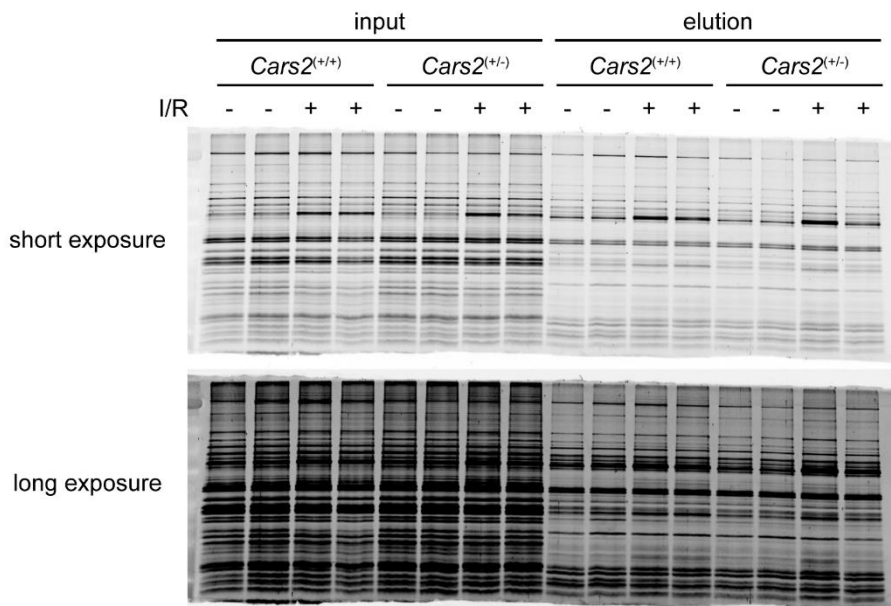
Figure 10. CARS2 heterozygous deficiency does not affect cardiac global protein polysulfidation levels.

A. Protocol for detection of polysulfidated proteins. **B.** Representative SDS-PAGE gel image of polysulfidated proteins isolated from $Cars2^{(+/+)}$ and $Cars2^{(+/-)}$ mouse hearts after I/R. Mice were exposed to 15 min ischemia followed by 24 hours reperfusion. The samples before reactions (input) and after reactions with IAA-biotin (elution) were loaded. $Cars2^{(+/+)}$ I/R(-) n=2; $Cars2^{(+/+)}$ I/R(+) n=2; $Cars2^{(+/-)}$ I/R(-) n=2; $Cars2^{(+/-)}$ I/R(+) n=2.
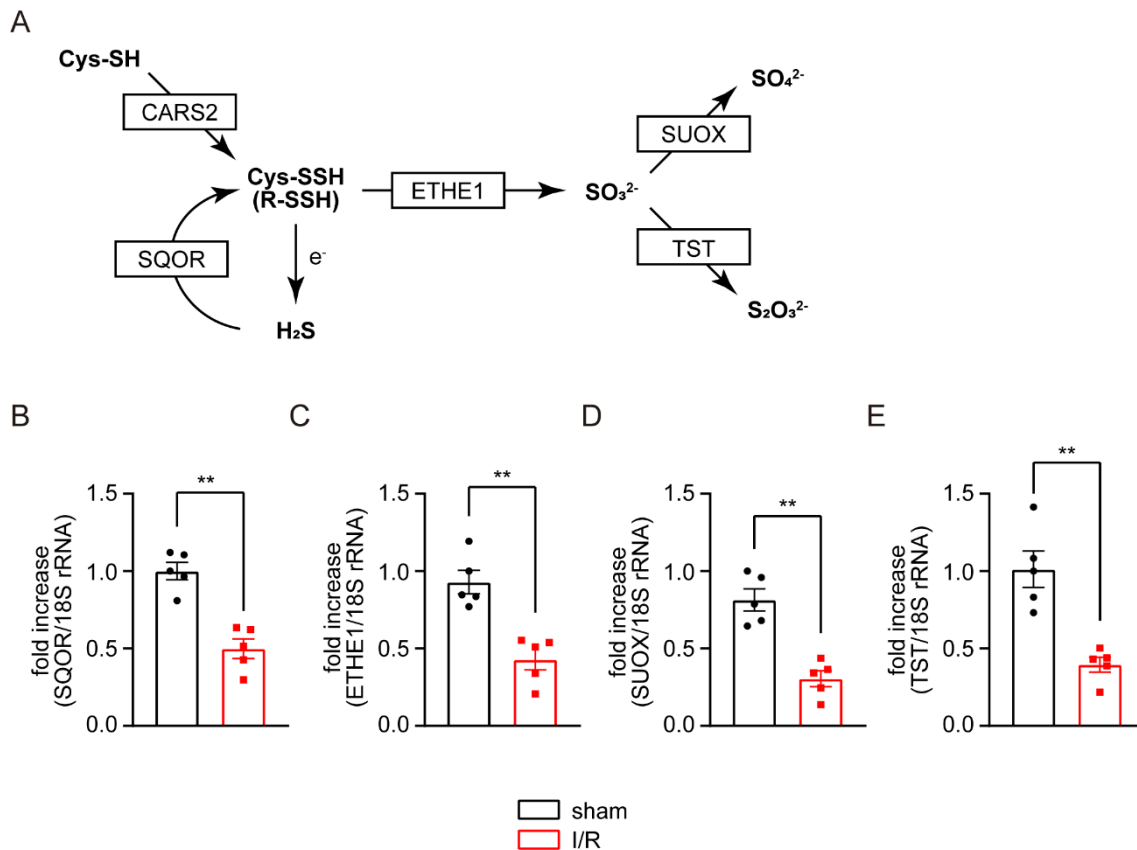
Figure 11. Changes in mRNA expression of RSS catabolizing enzymes in mouse hearts after I/R.

A. RSS metabolizing pathway. RSS are synthesized by CARS2. RSS can accept electrons and are reduced to H_2S. SQOR oxidizes H_2S and produces RSS. RSS are further oxidized by ETHE1 to sulfite (SO_3^{2-}). Sulfite is either oxidized to sulfate (SO_4^{2-}) by SUOX or to thiosulfate ($S_2O_3^{2-}$) by TST. **B, C, D, E.** The mRNA expression of RSS catabolizing enzymes including SQOR (B), ETHE1 (C), SUOX (D), and TST (E) were analyzed by qPCR. 15 min ischemia followed by 24 hours reperfusion was introduced. Sham n=5; I/R n=5. Data are shown as the means ± SEM. $^{**}P<0.01$ tested by t-test.

A

B

C
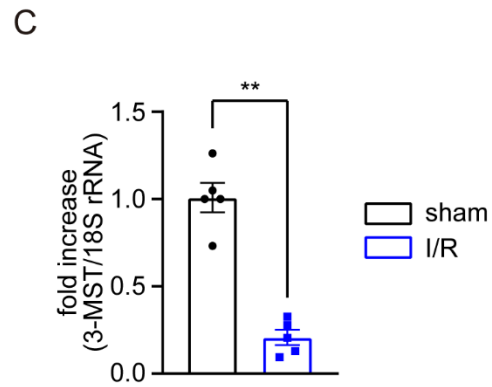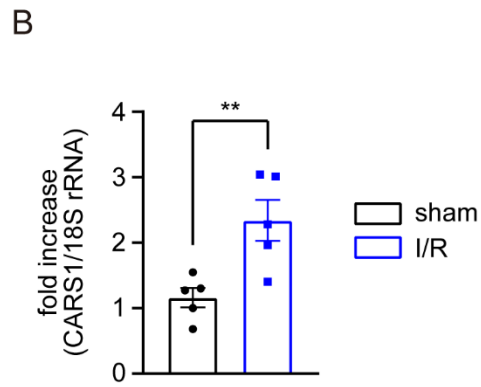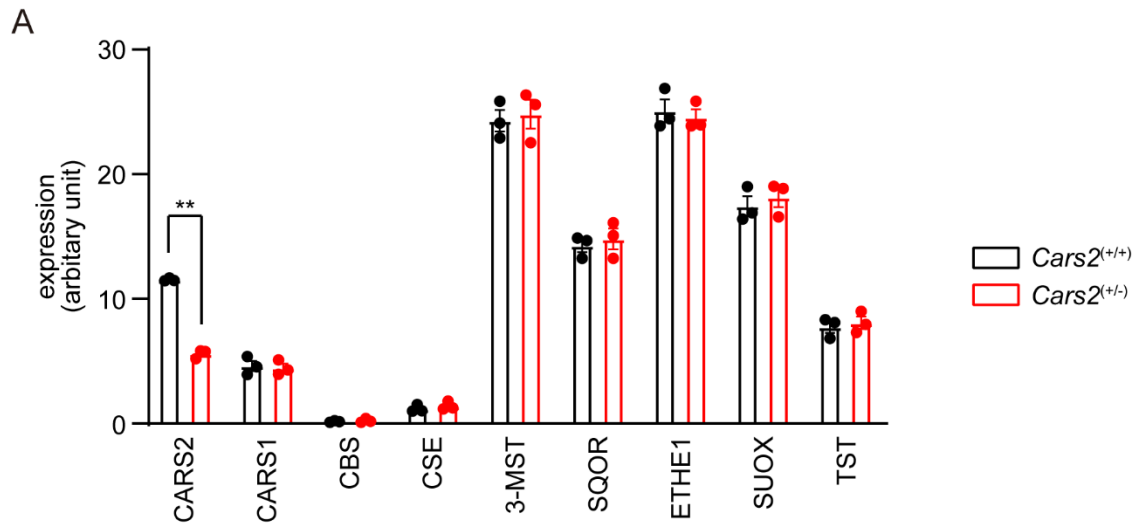
Figure 12. CARS1 mRNA level is compensatively increased in I/R-injured hearts.

A. The results of RNA-seq analysis for RSS metabolizing enzymes in *Cars2*[(+/+)] or *Cars2*[(+/-)] hearts. *Cars2*[(+/+)] n=3; *Cars2*[(+/-)] n=3. **B, C.** The expression of CARS1 (B) and 3-MST (C) mRNA were measured by qPCR. Mice were exposed to 15 min ischemia followed by 24 hours reperfusion. Sham n=5; I/R n=5. Data are shown as the means ± SEM. [**]$P<0.01$ tested by t-test.

Tables

	-SH form	-SSH form (RSS)
L-cysteine (Cys-SH)	8.29 [71,72]	4.34[* 71]
Glutathione (GSH)	8.94 [72]	5.45 [73]

Table 1. The proton dissociation constant (pKa) values of thiol (-SH) containing biological molecules and corresponding persulfides (-SSH).

[*]estimated parameter[71]

	sham vehicle (n=5)	sham cilnidipine (n=5)	MI vehicle (n=8)	MI cilnidipine (n=8)
IVSTd (mm)	1.00 ± 0.01	0.99 ± 0.03	$0.54 \pm 0.05^{**,\dagger\dagger}$	0.77 ± 0.09
LVIDd (mm)	2.82 ± 0.06	2.76 ± 0.07	$4.81 \pm 0.27^{**,\dagger\dagger}$	$4.35 \pm 0.15^{**,\dagger\dagger}$
LVPWd (mm)	0.99 ± 0.03	0.94 ± 0.03	0.95 ± 0.03	1.01 ± 0.03
LVIDs (mm)	1.17 ± 0.02	1.26 ± 0.10	$4.04 \pm 0.29^{**,\dagger\dagger}$	$3.33 \pm 0.19^{**,\dagger\dagger}$
HR (bpm)	505.40 ± 7.77	508.93 ± 14.37	483.75 ± 9.52	477.79 ± 8.10
EF (%)	92.34 ± 0.47	89.46 ± 1.80	$40.02 \pm 3.40^{**,\dagger\dagger}$	$53.40 \pm 3.16^{**,\dagger\dagger,\ddagger\ddagger}$
FS (%)	58.57 ± 0.85	54.49 ± 2.74	$16.65 \pm 1.67^{**,\dagger\dagger}$	$23.80 \pm 2.02^{**,\dagger\dagger,\ddagger}$

Table 2. Cardiac parameters of cilnidipine-treated MI mice (4 weeks after the surgery) measured by echocardiography.

IVSTd, interventricular septum thickness at diastole; LVIDd, left ventricular intra diameter at diastole; LVPWd, left ventricular posterior wall thickness at diastole; LVIDs; left ventricular intra diameter at systole; HR, heart rate; EF, ejection fraction; FS, fractional shortening. **P<0.01 vs sham vehicle, ††P<0.01 vs sham cilnidipine, ‡P<0.05, ‡‡P<0.01 vs MI vehicle tested by one-way ANOVA.

	MeHg(-) vehicle sham (n=5)	MeHg(-) vehicle TAC (n=6)	MeHg(-) NaHS sham (n=8)	MeHg(-) NaHS TAC (n=6)
IVSTd (mm)	0.98 ± 0.02	1.13 ± 0.04	1.00 ± 0.03	1.16 ± 0.08
LVIDd (mm)	2.69 ± 0.06	2.66 ± 0.06	2.81 ± 0.04	2.57 ± 0.06
LVPWd (mm)	0.94 ± 0.03	1.06 ± 0.04	0.96 ± 0.01	1.11 ± 0.04[‡, §]
LVIDs (mm)	1.20 ± 0.04	1.21 ± 0.05	1.27 ± 0.04	1.14 ± 0.04
HR (bpm)	565.80 ± 12.86	537.39 ± 8.07	550.13 ± 12.56	550.00 ± 12.47
EF (%)	90.43 ± 0.50	90.00 ± 0.59	89.96 ± 0.69	90.70 ± 0.77
FS (%)	55.72 ± 0.81	54.77 ± 0.94	54.69 ± 1.08	55.93 ± 1.33

	MeHg(+) vehicle sham (n=6)	MeHg(+) vehicle TAC (n=10)	MeHg(+) NaHS sham (n=6)	MeHg(+) NaHS TAC (n=8)
IVSTd (mm)	0.98 ± 0.03	1.20 ± 0.04$^{*, \dagger, \ddagger\ddagger}$	1.03 ± 0.03	1.18 ± 0.04‡
LVIDd (mm)	2.78 ± 0.07	2.78 ± 0.07	2.70 ± 0.05	2.70 ± 0.03
LVPWd (mm)	0.92 ± 0.02	1.10 ± 0.04$^{\dagger, \ddagger\ddagger, \S}$	0.94 ± 0.02	1.15 ± 0.04$^{**, \dagger\dagger, \ddagger\ddagger, \S\S}$
LVIDs (mm)	1.22 ± 0.05	1.45 ± 0.05$^{**, \ddagger, \S\S, aa, bb, c}$	1.21 ± 0.04	1.26 ± 0.03
HR (bpm)	499.50 ± 14.17$^{**, \dagger}$	541.13 ± 6.34	544.78 ± 9.46	521.50 ± 11.43
EF (%)	90.70 ± 0.70	84.69 ± 1.05$^{**, \dagger\dagger, \ddagger\ddagger, \S\S, aa, bb, cc}$	90.39 ± 0.70	89.11 ± 0.51
FS (%)	56.10 ± 1.11	47.75 ± 1.22$^{**, \dagger\dagger, \ddagger\ddagger, \S\S, aa, bb, cc}$	55.44 ± 1.22	53.43 ± 0.79

Table 3. Cardiac parameters of MeHg-exposed and NaHS-treated TAC mice (1 week after the surgery) measured by echocardiography.

IVSTd, interventricular septum thickness at diastole; LVIDd, left ventricular intra diameter at diastole; LVPWd, left ventricular posterior wall thickness at diastole; LVIDs; left ventricular intra diameter at systole; HR, heart rate; EF, ejection fraction; FS, fractional shortening. $^*P<0.05$, $^{**}P<0.01$ vs MeHg(-) vehicle sham, $^\dagger P<0.05$, $^{\dagger\dagger}P<0.01$ vs MeHg(-) NaHS sham, $^\ddagger P<0.05$, $^{\ddagger\ddagger}P<0.01$ vs MeHg(+) vehicle sham, $^\S P<0.05$, $^{\S\S}P<0.01$ vs MeHg(+) NaHS sham, $^{aa}P<0.01$ vs MeHg(-) vehicle TAC, $^{bb}P<0.01$ vs MeHg(-) NaHS TAC, $^c P<0.05$, $^{cc}P<0.01$ vs MeHg(+) NaHS TAC tested by one-way ANOVA.

	Cars2[(+/+)]	*Cars2*[(+/-)]
	(n=10)	(n=12)
4D mode		
volume;s (µL)	22.5 ± 1.1	23.1 ± 1.1
volume;d (µL)	48.8 ± 2.1	50.2 ± 2.7
SV (µL)	26.3 ± 1.3	27.1 ± 2.0
EF (%)	53.8 ± 1.4	53.6 ± 1.4
CO (mL/min)	11.3 ± 0.7	11.9 ± 1.1
HR (bpm)	429.2 ± 9.1	434.7 ± 12.2
M-mode		
IVS;d (mm)	0.7 ± 0.0	0.8 ± 0.0
LVID;d (mm)	3.9 ± 0.0	4.0 ± 0.1
LVPW;d (mm)	0.9 ± 0.0	1.0 ± 0.0

Table 4. Cardiac parameters of CARS2 KO mice measured by echocardiography.
volume;s, left ventricular systolic volume; volume;d, left ventricular diastolic volume;
SV, stroke volume; EF, ejection fraction; CO, cardiac output; HR, heart rate; IVS;d,
interventricular septum thickness at diastole; LVID;d, left ventricular intra diameter at
diastole; LVPW;d, left ventricular posterior wall thickness at diastole.

	Cars2$^{(+/+)}$ sham (n=5)	Cars2$^{(+/+)}$ I/R (n=5)	Cars2$^{(+/-)}$ sham (n=6)	Cars2$^{(+/-)}$ I/R (n=5)
volume;s (μL)	19.3 ± 1.5	25.1 ± 4.4	18.5 ± 1.5	93.7 ± 13.5[**, ††, ‡‡]
volume;d (μL)	40.9 ± 2.6	50.4 ± 4.5	41.7 ± 4.1	112.1 ± 14.6[**, ††, ‡‡]
SV (μL)	21.6 ± 1.6	25.2 ± 1.2	23.2 ± 3.1	18.4 ± 2.0
EF (%)	52.8 ± 2.0	51.6 ± 4.8	54.7 ± 3.2	17.1 ± 1.8[**, ††, ‡‡]
CO (mL/min)	10.3 ± 1.0	12.3 ± 1.1	11.1 ± 1.7	9.9 ± 1.1
HR (bpm)	478.0 ± 23.8	482.8 ± 24.6	476.9 ± 21.1	536.9 ± 8.6

Table 5. Cardiac parameters of CARS2 KO mice 7 days after I/R surgery measured by echocardiography.

volume;s, left ventricular systolic volume; volume;d, left ventricular diastolic volume; SV, stroke volume; EF, ejection fraction; CO, cardiac output; HR, heart rate. [**]$P<0.01$ vs Cars2$^{(+/+)}$ sham, [††]$P<0.01$ vs Cars2$^{(+/+)}$ I/R, [‡‡]$P<0.01$ vs Cars2$^{(+/-)}$ sham tested by one-way ANOVA.

Acknowledgements

References

1. Zhou, B. & Tian, R. Mitochondrial dysfunction in pathophysiology of heart failure. *J. Clin. Invest.* **128**, 3716–3726 (2018).

2. Garnier, A. *et al.* Depressed mitochondrial transcription factors and oxidative capacity in rat failing cardiac and skeletal muscles. *J. Physiol.* **551**, 491–501 (2003).

3. Mailloux, R. J., Jin, X. & Willmore, W. G. Redox regulation of mitochondrial function with emphasis on cysteine oxidation reactions. *Redox Biol.* **2**, 123–139 (2014).

4. Kirkinezos, I. G. & Moraes, C. T. Reactive oxygen species and mitochondrial diseases. *Semin. Cell Dev. Biol.* **12**, 449–457 (2001).

5. Ademowo, O. S., Dias, H. K. I., Burton, D. G. A. & Griffiths, H. R. Lipid (per) oxidation in mitochondria: an emerging target in the ageing process? *Biogerontology* **18**, 859–879 (2017).

6. Dorn, G. W. Mitochondrial fission/fusion and cardiomyopathy. *Curr. Opin. Genet. Dev.* **38**, 38–44 (2016).

7. Youle, R. J. & van der Bliek, A. M. Mitochondrial Fission, Fusion, and Stress. *Science (80-.).* **337**, 1062–1066 (2012).

8. Ikeda, Y. *et al.* Endogenous Drp1 mediates mitochondrial autophagy and protects the heart against energy stress. *Circ. Res.* **116**, 264–278 (2015).

9. Chen, Y., Liu, Y. & Dorn, G. W. Mitochondrial fusion is essential for organelle function and cardiac homeostasis. *Circ. Res.* **109**, 1327–1331 (2011).

10. Song, M., Franco, A., Fleischer, J. A., Zhang, L. & Dorn, G. W. Abrogating Mitochondrial Dynamics in Mouse Hearts Accelerates Mitochondrial Senescence. *Cell Metab.* **26**, 872-883.e5 (2017).

11. Nishimura, A. *et al.* Hypoxia-induced interaction of filamin with Drp1 causes mitochondrial hyperfission-associated myocardial senescence. *Sci. Signal.* **11**, (2018).

12. Nishimura, A. *et al.* Depolysulfidation of Drp1 induced by low-dose methylmercury exposure increases cardiac vulnerability to hemodynamic overload. *Sci. Signal.* (2019) doi:10.1126/scisignal.aaw1920.

13. Hu, Q. *et al.* Increased Drp1 acetylation by lipid overload induces cardiomyocyte death and heart dysfunction. *Circ. Res.* 456–470 (2020) doi:10.1161/CIRCRESAHA.119.315252.

14. Xu, X. H. *et al.* VEGF attenuates development from cardiac hypertrophy to heart failure after aortic stenosis through mitochondrial mediated apoptosis and cardiomyocyte proliferation. *J. Cardiothorac. Surg.* **6**, 1–9 (2011).

15. Kim, Y. M. *et al.* Redox Regulation of Mitochondrial Fission Protein Drp1 by Protein Disulfide Isomerase Limits Endothelial Senescence. *Cell Rep.* **23**, 3565–3578 (2018).

16. Cho, D.-H. *et al.* S-nitrosylation of Drp1 mediates beta-amyloid-related mitochondrial fission and neuronal injury. *Science (80-.).* **324**, 102–106 (2009).

17. Carvalho, C. M. L., Chew, E. H., Hashemy, S. I., Lu, J. & Holmgren, A. Inhibition of the human thioredoxin system: A molecular mechanism of mercury toxicity. *J. Biol. Chem.* **283**, 11913–11923 (2008).

18. Ekino, S., Susa, M., Ninomiya, T., Imamura, K. & Kitamura, T. Minamata disease revisited: An update on the acute and chronic manifestations of methyl mercury poisoning. *J. Neurol. Sci.* **262**, 131–144 (2007).

19. Guallar, E. *et al.* Mercury, Fish Oils, and the Risk of Myocardial Infarction. *N. Engl. J. Med.* **347**, 1747–1754 (2002).

20. Akaike, T. *et al.* Cysteinyl-tRNA synthetase governs cysteine polysulfidation and mitochondrial bioenergetics. *Nat. Commun.* **8**, (2017).

21. Shinkai, Y. & Kumagai, Y. Sulfane Sulfur in Toxicology: A Novel Defense System Against Electrophilic Stress. *Toxicological Sciences* (2019) doi:10.1093/toxsci/kfz091.

22. Toohey, J. I. Sulfur signaling: Is the agent sulfide or sulfane? *Anal. Biochem.* **413**, 1–7 (2011).

23. Kolluru, G. K., Shen, X. & Kevil, C. G. Reactive Sulfur Species: A New Redox Player in Cardiovascular Pathophysiology. *Arterioscler. Thromb. Vasc. Biol.* **40**, 874–884 (2020).

24. Ida, T. *et al.* Reactive cysteine persulfides and S-polythiolation regulate oxidative stress and redox signaling. *Proc. Natl. Acad. Sci. U. S. A.* **111**, 7606–7611 (2014).

25. Nishida, M. *et al.* Hydrogen sulfide anion regulates redox signaling via electrophile sulfhydration. *Nat. Chem. Biol.* **8**, 714–724 (2012).

26. Shimoda, K. *et al.* Modulation of P2Y6R expression exacerbates pressure overload-induced cardiac remodeling in mice. *Sci. Rep.* **10**, 1–11 (2020).

27. Oda, S. *et al.* TRPC6 counteracts TRPC3-Nox2 protein complex leading to attenuation of hyperglycemia-induced heart failure in mice. *Sci. Rep.* (2017) doi:10.1038/s41598-017-07903-4.

28. Kitajima, N. *et al.* TRPC3 positively regulates reactive oxygen species driving maladaptive cardiac remodeling. *Sci. Rep.* **6**, 1–14 (2016).

29. Numaga-Tomita, T. *et al.* TRPC3-GEF-H1 axis mediates pressure overload-induced cardiac fibrosis. *Sci. Rep.* (2016) doi:10.1038/srep39383.

30. Omatsu-Kanbe, M., Yoshioka, K., Fukunaga, R., Sagawa, H. & Matsuura, H. A simple antegrade perfusion method for isolating viable single cardiomyocytes from neonatal to aged mice. *Physiol. Rep.* **6**, 1–9 (2018).

31. Hausenloy, D. J. & Yellon, D. M. Myocardial ischemia-reperfusion injury: A neglected therapeutic target. *J. Clin. Invest.* **123**, 92–100 (2013).

32. Takano, Y. *et al.* Development of a reversible fluorescent probe for reactive sulfur species, sulfane sulfur, and its biological application. *Chem. Commun.* **53**, 1064–1067 (2017).

33. Fujii, S., Sawa, T., Motohashi, H. & Akaike, T. Persulfide synthases that are functionally coupled with translation mediate sulfur respiration in mammalian cells. *Br. J. Pharmacol.* **176**, 607–615 (2019).

34. Umezawa, K., Kamiya, M. & Urano, Y. A Reversible Fluorescent Probe for Real-Time Live-Cell Imaging and Quantification of Endogenous Hydropolysulfides. *Angew. Chemie - Int. Ed.* **57**, 9346–9350 (2018).

35. Lin, V. S., Lippert, A. R. & Chang, C. J. Cell-trappable fluorescent probes for endogenous hydrogen sulfide signaling and imaging H2O2-dependent H2S production. *Proc. Natl. Acad. Sci. U. S. A.* **110**, 7131–7135 (2013).

36. Landry, A. P., Ballou, D. P. & Banerjee, R. Hydrogen Sulfide Oxidation by Sulfide Quinone Oxidoreductase. *ChemBioChem* **22**, 949–960 (2021).

37. Kimura, Y. *et al.* Identification of H2S3 and H2S produced by 3-mercaptopyruvate sulfurtransferase in the brain. *Sci. Rep.* **5**, 1–11 (2015).

38. Porrello, E. R. *et al.* Transient Regenerative Potential of the Neonatal Mouse Heart. *Science (80-.).* **331**, 1078–1081 (2011).

39. Amoni, M. *et al.* Ventricular arrhythmias in ischemic cardiomyopathy—New avenues for mechanism-guided treatment. *Cells* **10**, 1–29 (2021).

40. Chandra, K. S. & Ramesh, G. The fourth-generation Calcium channel blocker: Cilnidipine. *Indian Heart J.* **65**, 691–695 (2013).

41. Nagai, H. *et al.* Cilnidipine, an N+L-type dihydropyridine Ca channel blocker, suppresses the occurence of ischemia/reperfusion arrhythmia in a rabbit model of myocardial infarction. *Hypertens. Res.* **28**, 361–368 (2005).

42. Luo, T. T. *et al.* Drp1 is widely, yet heterogeneously, distributed in the mouse central nervous system. *Mol. Brain* **13**, 1–22 (2020).

43. Riccio, M. P. *et al.* Bipolar disorder with Melnick–Needles syndrome and periventricular nodular heterotopia: two case reports and a review of the literature. *J. Med. Case Rep.* **15**, 1–5 (2021).

44. Burns, L. H. & Wang, H.-Y. Altered filamin A enables amyloid beta-induced tau hyperphosphorylation and neuroinflammation in Alzheimer's disease. *Neuroimmunol. Neuroinflammation* **4**, 263–271 (2017).

45. Oliver, D. & Reddy, P. H. Dynamics of Dynamin-Related Protein 1 in Alzheimer's Disease and Other Neurodegenerative Diseases. *Cells* **8**, 1–20 (2019).

46. Farina, M., Rocha, J. B. T. & Aschner, M. Mechanisms of methylmercury-induced neurotoxicity: evidence from experimental studies. *Life Sci.* **89**, 555–563 (2011).

47. Kerper, L. E., Ballatori, N. & Clarkson, T. W. Methylmercury transport across the blood-brain barrier by an amino acid carrier. *Am. J. Physiol. - Regul. Integr. Comp. Physiol.* **262**, (1992).

48. Fujii, S. *et al.* The critical role of nitric oxide signaling, via protein S-guanylation and nitrated cyclic GMP, in the antioxidant adaptive response. *J. Biol. Chem.* **285**, 23970–23984 (2010).

49. Sawa, T. *et al.* Protein S-guanylation by the biological signal 8-nitroguanosine 3′,5′-cyclic monophosphate. *Nat. Chem. Biol.* **3**, 727–735 (2007).

50. Khan, S. *et al.* Reactive Persulfides from Salmonella Typhimurium

Downregulate Autophagy-Mediated Innate Immunity in Macrophages by Inhibiting Electrophilic Signaling. *Cell Chem. Biol.* **25**, 1403-1413.e4 (2018).

51. Sorokin, D. Y. *et al.* Elemental sulfur and acetate can support life of a novel strictly anaerobic haloarchaeon. *ISME J.* **10**, 240–252 (2016).

52. Toohey, J. I. & Cooper, A. J. L. Thiosulfoxide (Sulfane) sulfur: New chemistry and new regulatory roles in biology. *Molecules* **19**, 12789–12813 (2014).

53. Pandey, A. *et al.* Mitochondria Export Sulfur Species Required for Cytosolic tRNA Thiolation. *Cell Chem. Biol.* **25**, 738-748.e3 (2018).

54. Marutani, E. *et al.* Sulfide catabolism ameliorates hypoxic brain injury. *Nat. Commun.* **12**, (2021).

55. Tiranti, V. *et al.* Loss of ETHE1, a mitochondrial dioxygenase, causes fatal sulfide toxicity in ethylmalonic encephalopathy. *Nat. Med.* **15**, 200–205 (2009).

56. Ergene, M. *et al.* Severe isolated sulfide oxidase deficiency with a novel mutation. *Turk. J. Pediatr.* **63**, 716–720 (2021).

57. Claerhout, H. *et al.* Isolated sulfite oxidase deficiency. *J. Inherit. Metab. Dis.* **41**, 101–108 (2018).

58. Morton, N. M. *et al.* Genetic identification of thiosulfate sulfurtransferase as an adipocyte-expressed antidiabetic target in mice selected for leanness. *Nat. Med.* **22**, 771–779 (2016).

59. Carter, R. N. *et al.* The hepatic compensatory response to elevated systemic sulfide promotes diabetes. *Cell Rep.* **37**, 109958 (2021).

60. Rajpal, S. *et al.* Total sulfane sulfur bioavailability reflects ethnic and gender disparities in cardiovascular disease. *Redox Biol.* **15**, 480–489 (2018).

61. Calvert, J. W. *et al.* Genetic and pharmacologic hydrogen sulfide therapy attenuates ischemia-induced heart failure in mice. *Circulation* (2010) doi:10.1161/CIRCULATIONAHA.109.920991.

62. Pedre, B. & Dick, T. P. 3-Mercaptopyruvate sulfurtransferase: An enzyme at the crossroads of sulfane sulfur trafficking. *Biol. Chem.* **402**, 223–237 (2021).

63. Peleli, M. *et al.* Cardiovascular phenotype of mice lacking 3-mercaptopyruvate sulfurtransferase. *Biochem. Pharmacol.* **176**, (2020).

64. Yu, L. *et al.* Diallyl trisulfide exerts cardioprotection against myocardial ischemia-reperfusion injury in diabetic state, role of AMPK-mediated

AKT/GSK-3β/HIF-1α activation. *Oncotarget* **8**, 74791–74805 (2017).

65. Predmore, B. L. *et al.* The polysulfide diallyl trisulfide protects the ischemic myocardium by preservation of endogenous hydrogen sulfide and increasing nitric oxide bioavailability. *Am. J. Physiol. - Hear. Circ. Physiol.* **302**, 2410–2418 (2012).

66. Shen, Y., Shen, Z., Luo, S., Guo, W. & Zhu, Y. Z. The cardioprotective effects of hydrogen sulfide in heart diseases: From molecular mechanisms to therapeutic potential. *Oxid. Med. Cell. Longev.* **2015**, (2015).

67. Luan, H. F. *et al.* Hydrogen sulfide postconditioning protects isolated rat hearts against ischemia and reperfusion injury mediated by the JAK2/STAT3 survival pathway. *Brazilian J. Med. Biol. Res.* **45**, 898–905 (2012).

68. Elrod, J. W. *et al.* Hydrogen sulfide attenuates myocardial ischemia-reperfusion injury by preservation of mitochondrial function. *Proc. Natl. Acad. Sci. U. S. A.* (2007) doi:10.1073/pnas.0705891104.

69. Ishigami, M. *et al.* A source of hydrogen sulfide and a mechanism of its release in the brain. *Antioxidants Redox Signal.* **11**, 205–214 (2009).

70. Wang, Y. *et al.* SLC25A39 is necessary for mitochondrial glutathione import in mammalian cells. *Nature* **599**, (2021).

71. Cuevasanta, E. *et al.* Reaction of Hydrogen Sulfide with Disulfide and Sulfenic Acid to Form the Strongly Nucleophilic Persulfide. *J. Biol. Chem.* **290**, 26866–26880 (2015).

72. Portillo-ledesma, S. *et al.* Deconstructing the Catalytic Efficiency of Peroxiredoxin-5 Peroxidatic Cysteine. *Biochemistry* **53**, 6113–6125 (2014).

73. Benchoam, D. *et al.* Acidity and nucleophilic reactivity of glutathione persulfide. *J. Biol. Chem.* **295**, 15466–15481 (2020).